Beam Dynamics of Collective Instabilities in High-Energy Accelerators

A. Chao
SLAC National Accelerator Laboratory, Menlo Park, United States

Abstract

This lecture provides an abbreviated overview of the basic physics of collective instabilities of intense charged particle beams in high-energy accelerators.

Keywords

Collective instabilities, Gauss's law, impedance, Landau damping, Vlasov equation, wakefield

1 Gauss's law

Collective instabilities in accelerators mostly come from an intense charged particle beam electromagnetically interacting with its vacuum chamber environment. As the beam interacts with its environment, it generates an electromagnetic field called the *wakefield*, and the wakefield acts back on the beam, disturbing its motion; if the perturbation is strong enough, the beam becomes unstable.

To discuss the wakefield, we must start with its ultimate origin, *Gauss's law*, which states that each charged particle always has a definite amount of electric field lines attached to it. We can distort these field lines but we can never cut them loose from the charge under any circumstances. Furthermore, the amount of field lines attached to each charge can never be changed, neither increased nor decreased.

Gauss's law is amazing. Mathematically, it reads

$$\nabla \cdot \vec{E} = 4\pi\rho \ .$$

Physically it reads: electric field lines are absolutely attached to the charges.

The integral form of Gauss's law is

$$\oint_S \vec{E} \cdot \mathrm{d}\vec{S} = 4\pi Q \ ,$$

where Q is the total charge inside the volume enclosed by the surface S. It is amazing that this law holds no matter how the charges are moving – non-relativistically, relativistically, or under acceleration, or whether they are embedded in any type of material. It also does not matter how close the charges might be immediately next to the surface S. The field integral will make a sudden change when a charge crosses the surface even infinitesimally.

2 A moving charge

If the charge is stationary and if it is in a free space, its field lines are as shown in Fig. 1(a). For a moving charge, we see Fig. 1(b). When v approaches c, we have Fig. 1(c), when all the electric fields stay in an infinitely thin sheet as result of the theory of relativity. For most accelerators, case (c) is closest to the case under consideration.

When the charge is moving, it also generates a magnetic field. This magnetic field also contracts to a thin pancake when $v = c$. The direction of the electric field is radial; the direction of the magnetic field is azimuthal (right-hand rule):

$$E_r \quad = \quad \frac{2q}{r}\delta(z - ct) \ ,$$
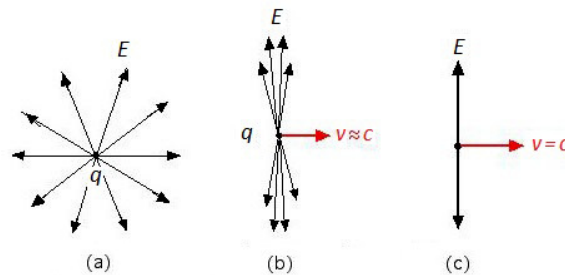
Fig. 1: Electric field lines of a charge: (a) stationary; (b) moving relativistically; (c) when $v = c$
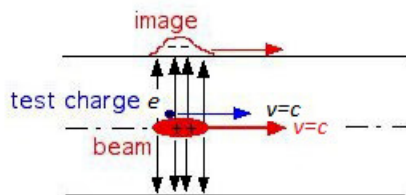
Fig. 2: Ultrarelativistic beam going down perfectly conducting smooth vacuum pipe

$$B_\theta \quad = \quad \frac{2q}{r}\delta(z - ct) \ .$$

One observes that

$$B_\theta = E_r \quad \text{when} \quad v = c \ .$$

However, when $v = 0$, there is no magnetic field. When v increases, B_θ increases, but is still weaker than E_r. Only when $v = c$ do we have $B_\theta = E_r$. The fact that $B_\theta = E_r$ when $v = c$ has important consequences, as explained next.

3 The vacuum chamber

We now add the vacuum chamber. Consider a very smooth vacuum chamber beam pipe. (How smooth does the chamber have to be? A 1 mm discontinuity on the pipe is considered a potential problem. In some circumstances, a 1 μm roughness on the wall surface can have a significant effect.) Consider the smooth pipe wall to be perfectly conducting.

The ultrarelativistic beam going down the axis of the pipe, together with its electromagnetic field and the smooth vacuum chamber, is as shown in Fig. 2.

The electromagnetic fields are perfectly and cleanly terminated on the pipe wall. No fields penetrate into the wall because it is a perfect conductor. The image charge on the wall is exactly equal and opposite to that of the beam, and it also moves with $v = c$ (except that this is phase velocity, not group velocity). The entire field pattern moves with the beam. There is no wakefield.

Is this beam stable? Consider a particular particle in the beam, the 'test particle' e in Fig. 2. This test particle will see an electric force $e\vec{E}$ due to the electric field carried by the beam. This force is easily seen to push e towards the vacuum chamber wall because the test charge e has the same sign as the charges of the beam.

But there is also a magnetic force. The magnetic field is in the azimuthal direction (right-hand rule). The magnetic force is $(e/c)\,\vec{v} \times \vec{B}$. It is easily seen that this magnetic force is pointing towards the pipe axis.
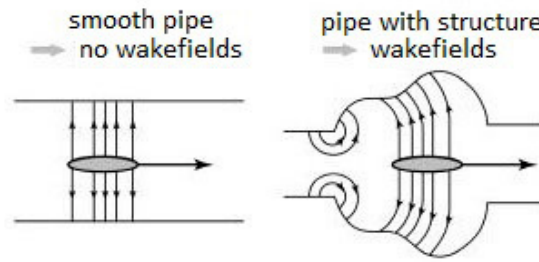
Fig. 3: Discontinuities generate wakefields

We mentioned that when $v = c$, we have $E_r = B_\theta$. In the ultrarelativistic limit, therefore, the electric and the magnetic forces exactly cancel. The particles in the ultrarelativistic beam see the electric force and magnetic force, but they do not see a net force. The collective electromagnetic fields carried by the beam do not influence particle motion. There are no collective instabilities.

This cancellation between the electric and magnetic forces due to the beam's self fields is very fortunate and very important. Without this cancellation, no modern accelerators would have worked.

We conclude that there are three possible ways for a collective instability to occur:

1. the beam is not relativistic enough;
2. the vacuum chamber is too resistive;
3. the vacuum chamber is not smooth enough.

If none of these apply, the beam is stable as just illustrated. If any one of these conditions occurs, the exact cancellation of the electric and magnetic forces is disrupted, and the beam can encounter an instability.

We construct accelerators to be as close to the cancellation condition as possible. The electric and magnetic forces generally cancel to high accuracy by design. However, the cancellation is never perfect. Vacuum chambers made of copper or aluminium are not perfectly conducting. There will be many small necessary discontinuities along the vacuum chamber pipe; beam position monitors, vacuum pumping ports, etc. There are also big discontinuities known as RF cavities. As to the condition of $v = c$, it is never satisfied completely. So the cancellation of electric and magnetic forces is not perfect. And that residual non-cancellation leads to collective instabilities.

4 Wakefields due to discontinuities

When a beam traverses a discontinuity, an electromagnetic wakefield is generated. An intense beam will generate a strong wakefield (Fig. 3). When the wakefield becomes too strong, the beam becomes unstable.

A wakefield is generated because the beam's image charges now have to move around a corner when encountering a discontinuity. Wakefields are the radiation fields of the image charges when their apparent trajectories are bent. (These are apparent trajectories. Image charges do not physically move along the wall surface.)

Once we accept that wakefields are a result of radiation, then just as with any other radiation, it is natural to ask about the frequency content of these wakefields. The answer is that it depends on the details of the beam and the detailed geometry of the discontinuity. In general, it covers a wide range, with wavelengths varying from micrometres to metres. To describe the frequency content of the wakefields, we introduce a quantity called *impedance*. Impedance is essentially the Fourier transform of wakefield.
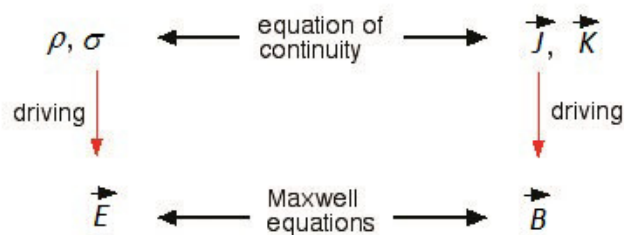
Fig. 4: Definition of metal: $\rho = 0$, $\vec{J} = \sigma\vec{E}$; definition of insulator: $\vec{J} = \vec{0}$, $\rho = \epsilon\nabla \cdot \vec{E}$

5 Wakefield due to a resistive wall

To discuss the resistive wall wakefield, let us first review the structure of electromagnetism by consulting Fig. 4. We note a clear symmetry between the electric family and the magnetic family in this chart. This symmetry, however, only holds in vacuum. It is lost when we consider a metal or an insulator. Metals break the symmetry by making a preference to the magnetic family $(\vec{B}, \vec{J})$, while insulators make a preference in favour of the electric family $(\vec{E}, \rho)$. No charges are allowed inside a metal while currents are allowed to penetrate. Inside a metal, therefore, there is more magnetic field than electric field. Conversely, currents are not allowed inside an insulator, and there is more electric field than magnetic field.

In the case of a wall of resistive metal, the wakefield is generated by the following physical process.

1. When the beam's image charges flow on the vacuum chamber wall, the electric field carried by the point charge will be terminated immediately by the image charges on the wall surface, while the magnetic field carried by the point charge is mostly cancelled by the image current on the wall surface, but this cancellation is not exact because the current has penetrated the wall by a skin depth.

2. As the image current slowly resurfaces after the point charge has passed by, this resurfacing image current drives new magnetic fields. These new magnetic fields occur after the point charge has left.

3. The resurfacing current and magnetic field will execute some transient behaviour, and quickly oscillate a few times. After the initial transient, the resurfacing current and magnetic field decays away but at a very slow rate.

4. The resurfacing changing magnetic field now drives an electric field (Maxwell's equation). This yields some electric field inside the resistive wall after all, but this electric field is very weak.

For the case of a resistive wall pipe with circular cross-section, and an ultrarelativistic point charge q going down its axis, Fig. 5 shows the electric component of the wakefield inside the vacuum chamber. Note that there is also a matching magnetic field pattern, and that both the electric and magnetic field patterns follow the leading point charge as a frozen pattern, indicating a phase velocity of c, but it is important to know that the wakefield energy flows not purely in the forward direction with the speed of light. Underneath this apparent frozen energy flow is an important flow of energy from the point charge q towards to wall surface to be deposited as wall heating.

The quantity χ that enters the horizontal axis is a small dimensionless parameter defined by

$$\chi = \frac{c}{4\pi\sigma b} \, ,$$

with b the vacuum pipe radius and σ the conductivity of the pipe material. For example, if $b = 5$ cm and the wall is made of aluminium, $\chi = 1.5 \times 10^{-9}$. Note that we have used cgs units, in which conductivity can be converted by applying $1\,\Omega^{-1}\mathrm{m}^{-1} = 0.9 \times 10^{10}\mathrm{s}^{-1}$.
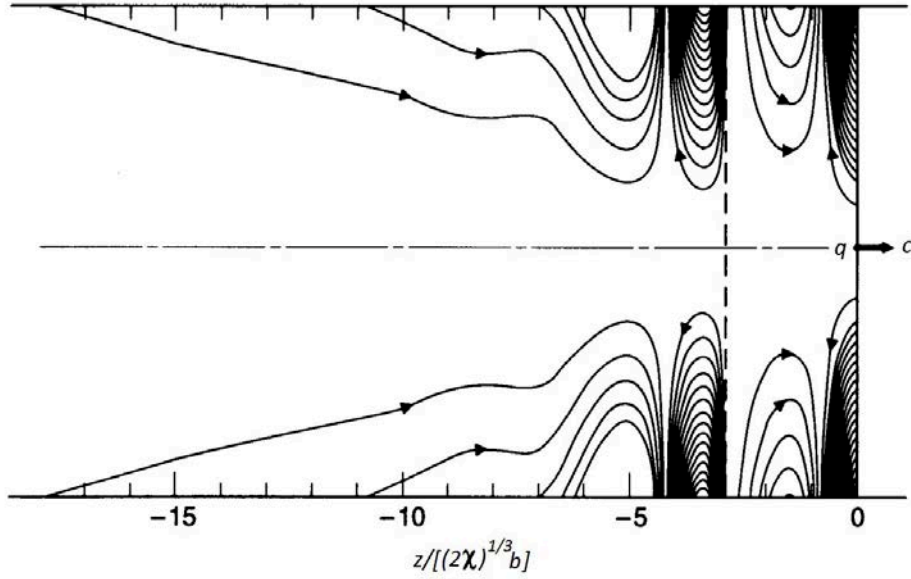
Fig. 5: Electric component of the wakefield inside the vacuum chamber for a resistive wall pipe with circular cross-section. The field line density is increased by a factor of 40 to the left of the dotted line.

As shown in Fig. 5, there is no wakefield ahead of the point charge, as causality would dictate. The wakefield pattern following the point charge is measured along distance z in units of $b(2\chi)^{1/3}$. Since $\chi \ll 1$, the resistive wall wakefield decays very quickly following the passage of the point charge.

However, after the quick initial decay, at long distances, the remaining resistive wall wake starts to decay very slowly. This means that the resistive wall wakefield has a long tail. An intense beam bunch, for example, can leave a wakefield that lasts long enough to affect its motion when the bunch returns after making one complete circuit around a circular accelerator.

As will be shown later, the fact that the resistive wall generates both short- and long-range wakefields is reflected by the fact that its corresponding impedance has an exceptionally wide spectrum, ranging from very short to very long wavelengths.

6 What happens to particle motion when there are wakefields?

Consider a beam with distribution ψ in phase space $(\vec{q}, \vec{p})$. The dynamics of the evolution of ψ are described by the Vlasov equation (see later),

$$\frac{\partial \psi}{\partial t} + \frac{\vec{p}}{m} \cdot \frac{\partial \psi}{\partial \vec{q}} + \vec{f} \cdot \frac{\partial \psi}{\partial \vec{p}} = 0 \,,$$

where

$$\vec{f} = e \left(\vec{E} + \frac{\vec{v}}{c} \times \vec{B} \right) \,,$$
$$\vec{E} = \vec{E}_{\text{ext}} + \vec{E}_{\text{wake}} \,,$$
$$\vec{B} = \vec{B}_{\text{ext}} + \vec{B}_{\text{wake}} \,.$$

The wakefields are determined by Maxwell's equations, where the source terms ρ and $\vec{j}$ are determined by the beam distribution ψ,

$$\rho = \int \mathrm{d}^3 p \, \psi \,, \qquad \vec{j} = \int \mathrm{d}^3 p \, \vec{v} \psi \,.$$
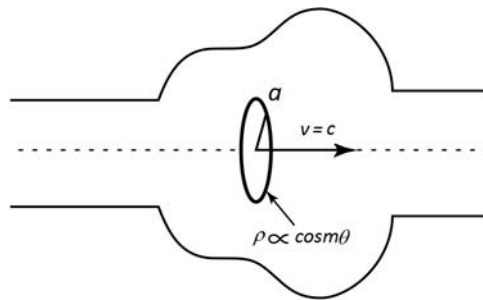
Fig. 6: We only need to calculate the wakefields generated by a rigid $\cos m\theta$ ring beam

We therefore have the situation when the beam distribution is described by the Vlasov equation whose force terms are given by the electromagnetic fields, while the electromagnetic fields are described by Maxwell's equations, whose source terms are given by the beam distribution. It is clear that a full treatment of the beam–wakefield system involves solving a coupled 'Vlasov–Maxwell equation'.

Beam–structure interaction is a difficult problem in general. It often requires numerical solution using particle-in-cell codes with demanding boundary conditions. Applying particle-in-cell codes is reasonable for small devices such as electron guns and klystrons, but becomes impractical for large accelerators.

So, can we simplify the problem for our purpose while maintaining sufficiently accurate results? Yes, we can. For *high-energy* accelerators, this complication can be avoided by using two simplifying approximations. These simplifications lead to the concepts of 'wake function' and 'impedance'.

1. Rigid-beam approximation:
   The first simplification is the rigid-beam approximation. At high energies, beam motion is affected little during the passage of a structure. This means that one can calculate the wakefields assuming the beam shape is rigid and its motion is ultrarelativistic with $v = c$. In fact, we only need to calculate the wakefields generated by a 'rigid $\cos m\theta$ ring beam' (Fig. 6). The wakefield of a general beam can be obtained by superposition.

2. Impulse approximation:
   The second simplification is the impulse approximation. We don't need to know $\vec{E}$ or $\vec{B}$ separately; we only need to know $\vec{f}$. For high energies, we don't even need the instantaneous $\vec{f}$. We only need the integrated impulse:

$$\Delta\vec{p} = \int_{-\infty}^{\infty} \mathrm{d}t\, \vec{f}.$$

   Figure 7 shows the configuration of a ring beam and a test charge that follows it. The ring beam generates a wakefield. The test charge receives a wake-induced impulse in the impulse approximation.

As we will see, these two approximations drastically simplify the problem at hand, thus allowing us to treat large accelerators with complicated boundary conditions without invoking particle-in-cell codes.

7 The Panofsky–Wenzel theorem

The instantaneous wakefields are complicated; fortunately, $\Delta\vec{p}$ is much simpler and, at high energies, it is $\Delta\vec{p}$ that we need. The Panofsky–Wenzel theorem applies to $\Delta\vec{p}$. It is the basis of all beam instability analyses in high energy accelerators. In comparison, the particle-in-cell codes aim to calculate the instantaneous wakefields in all their gory details, so are inefficient for our purpose.
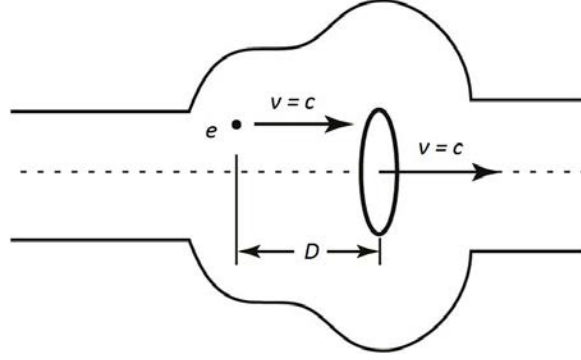
Fig. 7: A ring beam and a test charge that follows it

Maxwell's equations read

$$\nabla \cdot \vec{E} = 4\pi\rho \,,$$

$$\nabla \times \vec{B} - \frac{1}{c}\frac{\partial \vec{E}}{\partial t} = 4\pi\beta\rho\hat{z} \,,$$

$$\nabla \cdot \vec{B} = 0 \,,$$

$$\nabla \times \vec{E} + \frac{1}{c}\frac{\partial \vec{B}}{\partial t} = 0 \,,$$

where we have made the important rigid-beam approximations, $\vec{j} = \rho\vec{v}$ and $\vec{v} = \beta c\hat{z}$.

The Lorentz force as seen by the rigid test charge e is given by

$$\vec{f} = e(\vec{E} + \beta\hat{z} \times \vec{B}) \,.$$

Both the beam and the test charge move with $\vec{v} = \beta c\hat{z}$. The impulse is

$$\Delta\vec{p}(x, y, D) = \int_{-\infty}^{\infty} dt\, \vec{f}(x, y, D + \beta ct, t) \,.$$

Several important conditions can be found using Maxwell's equations. One of these is the Panofsky–Wenzel theorem. Without giving the derivation, it reads

$$\nabla \times \Delta\vec{p} = \vec{0} \,.$$

One can decompose the Panofsky–Wenzel theorem into a component parallel to $\hat{z}$ and a component perpendicular to $\hat{z}$, to obtain

$$\nabla \cdot (\hat{z} \times \Delta\vec{p}) = 0 \,, \tag{1}$$

$$\frac{\partial}{\partial D}\Delta\vec{p}_\perp = \nabla_\perp \Delta p_z \,. \tag{2}$$

Equation (1) says something about the transverse components of $\Delta\vec{p}$. Equation (2) says that the transverse gradient of the longitudinal wake impulse is equal to the longitudinal gradient of the transverse wake impulse.

Another important condition valid when $\beta = 1$ is

$$\nabla_\perp \cdot \Delta\vec{p}_\perp = 0 \,. \tag{3}$$

It is clear that the Panofsky–Wenzel theorem imposes strong constraints on the impulse received by a test charge from a relativistic beam.

8 Cylindrically symmetric pipe

In cylindrical coordinates, Eq. (1) gives

$$\nabla \cdot [\hat{z} \times (\Delta p_r \hat{r} + \Delta p_\theta \hat{\theta})] = 0$$

$$\implies \qquad \frac{\partial}{\partial r}(r\Delta p_\theta) = \frac{\partial}{\partial \theta}\Delta p_r \ .$$

Equation (2) gives

$$\frac{\partial}{\partial D}(\Delta p_r \hat{r} + \Delta p_\theta \hat{\theta}) = \left(\hat{r}\frac{\partial}{\partial r} + \frac{\hat{\theta}}{r}\frac{\partial}{\partial \theta}\right)\Delta p_z$$

$$\implies \qquad \begin{cases} \frac{\partial}{\partial D}\Delta p_r = \frac{\partial}{\partial r}\Delta p_z \\ \frac{\partial}{\partial D}\Delta p_\theta = \frac{1}{r}\frac{\partial}{\partial \theta}\Delta p_z \ . \end{cases}$$

Equation (3) gives

$$\frac{1}{r}\frac{\partial}{\partial r}(r\Delta p_r) + \frac{1}{r}\frac{\partial}{\partial \theta}\Delta p_\theta = 0$$

$$\implies \qquad \frac{\partial}{\partial r}(r\Delta p_r) = -\frac{\partial}{\partial \theta}\Delta p_\theta \qquad (\beta = 1) \ .$$

These results are surprisingly simple and general. They do not contain any beam source terms. The exact shape or distribution of the beam does not matter. Neither do these results depend on the boundary conditions. The boundary can be perfectly conducting or resistive metal, or it can be a dielectric. It does not have to be a sharply defined surface; it can, for example, be a gradually fading plasma surface. The only inputs needed are Maxwell's equations and the rigid-beam and impulse approximations.

We are now ready to consider a $\cos m\theta$ ring beam with $\vec{v} = c\hat{z}$ as we set out to solve Eqs. (1)–(3). The solution can be expressed in terms of a function $W_m(D)$, such that

$$c\Delta\vec{p}_\perp = -eI_m W_m(D)mr^{m-1}(\hat{r}\cos m\theta - \hat{\theta}\sin m\theta) \ ,$$
$$c\Delta p_z = -eI_m W'_m(D)r^m \cos m\theta \ , \qquad (4)$$

where I_m is the mth multipole moment of the ring beam, $W_m(D)$ is the transverse wake function and $W'_m(D)$ is the longitudinal wake function. The longitudinal wake function is simply the derivative of the transverse wake function.

Equation (4) contains explicit dependences on r and θ. The fact that we can go so far without any specific details is surprising and shows the power of this line of analysis. The dependence on D is through $W_m(D)$, which can be obtained only if boundary conditions are invoked.

When the beam pipe is cylindrically symmetrical, each m-multipole component of the beam excites a wake pattern according to Eq. (4). Different m components do not mix.

9 Decomposing wakefields into modes

Armed with the Panofsky–Wenzel theorem, to analyse the instability problem, we proceed as follows. We first consider the beam to be a δ-function in z. If the beam has a finite length, the result can be obtained by superposition.

We next decompose the transverse distribution into 'modes' and consider a single transverse mode m. A general transverse distribution can be obtained by superposition with a summation over m.

So the problem is now reduced to finding the impulse integrated by a test charge that is trailing behind a beam slice with a transverse mth moment I_m moving along the pipe axis. In this configuration,
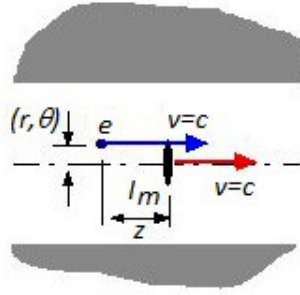
Fig. 8: A test charge trailing behind a beam slice with a transverse mth moment I_m moving along the pipe axis

Table 1: mth multipole wakefields

m	Distribution moments of beam	Longitudinal wake impulse	Transverse wake impulse
0	q	$-eq\,W_0'(z)$	0
1	$\begin{cases} q\langle x\rangle \\ q\langle y\rangle \end{cases}$	$-eq\langle x\rangle x W_1'(z)$ $-eq\langle y\rangle y W_1'(z)$	$-eq\langle x\rangle W_1(z)\hat{x}$ $-eq\langle y\rangle W_1(z)\hat{y}$
2	$\begin{cases} q\langle x^2-y^2\rangle \\ q\langle 2xy\rangle \end{cases}$	$-eq\langle x^2-y^2\rangle(x^2-y^2)W_2'(z)$ $-eq\langle 2xy\rangle 2xy\,W_2'(z)$	$-2eq\langle x^2-y^2\rangle W_2(z)(x\hat{x}-y\hat{y})$ $-2eq\langle 2xy\rangle W_2(z)(y\hat{x}+x\hat{y})$
3	$\begin{cases} q\langle x^3-3xy^2\rangle \\ q\langle 3x^2y-y^3\rangle \end{cases}$	$-eq\langle x^3-3xy^2\rangle$ $\times(x^3-3xy^2)W_3'(z)$ $-eq\langle 3x^2y-y^3\rangle$ $\times(3x^2y-y^3)W_3'(z)$	$-3eq\langle x^3-3xy^2\rangle W_3(z)$ $\times[(x^2-y^2)\hat{x}-2xy\hat{y}]$ $-3eq\langle 3x^2y-y^3\rangle W_3(z)$ $\times[2xy\hat{x}+(x^2-y^2)\hat{y}]$

as shown in Fig. 8, I_m is the driving beam, e is the test charge, z is the longitudinal distance by which e is trailing behind I_m, and (r,θ) is the transverse displacement of the test charge relative to the pipe axis.

For a cylindrical pipe, the mth multipole wakefield is driven when and only when the driving beam has an mth moment (Table 1).

In most applications, we care mostly about the $m=0$ monopole mode when discussing longitudinal collective instabilities and about the $m=1$ dipole mode when discussing transverse collective instabilities. Therefore, we mostly ask for $W_0(z)$ and $W_1(z)$. The reason $W_0(z)$ is not relevant for transverse instabilities is that the transverse impulse vanishes when $m=0$ for cylindrically symmetrical pipes.

The wakefield impulses have simple patterns—instantaneous wakefields do not share this simplicity. The $m=0$ and $m=1$ patterns are illustrated in Fig. 9.

10 Impedances

We mentioned that the wakefield wavelengths cover a wide range, from ~ 1 μm to ~ 1 m. What characterize the frequency content of the wakefields are the impedances, the Fourier transforms of the wake functions,

$$Z_m^{\|}(\omega) = \int\limits_{-\infty}^{\infty} \frac{\mathrm{d}z}{c} \mathrm{e}^{-\mathrm{i}\omega z/c}\, W_m'(z)\,, \tag{5}$$
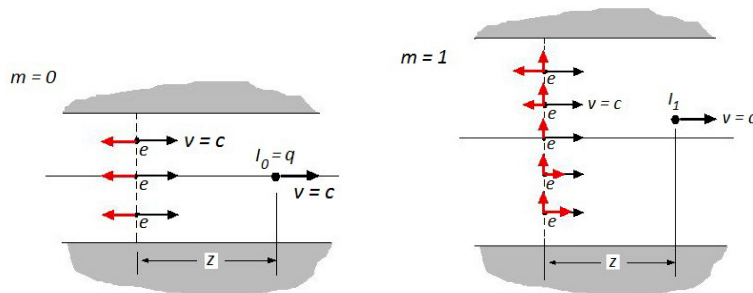
Fig. 9: $m = 0$ and $m = 1$ wakefield impulse patterns

$$Z_m^\perp(\omega) = i \int\limits_{-\infty}^{\infty} \frac{dz}{c} e^{-i\omega z/c}\, W_m(z) \,.$$

Since we have already discussed the wake functions, we consider Eq. (5) the definition of impedances.

Instead of wake functions, an accelerator designer therefore could ask about the impedance of the accelerator. The impedance is the quantity most directly related to the maximum beam current allowed by the accelerator. Inverting the Fourier transforms, we have

$$W_m'(z) = \frac{1}{2\pi} \int\limits_{-\infty}^{\infty} d\omega\, e^{i\omega z/c}\, Z_m^\parallel(\omega) \,,$$

$$W_m(z) = \frac{-i}{2\pi} \int\limits_{-\infty}^{\infty} d\omega\, e^{i\omega z/c}\, Z_m^\perp(\omega) \,.$$

The Panofsky–Wenzel theorem, which relates the longitudinal wake function to the derivative of the transverse wake function, also gives a relationship between the longitudinal and transverse impedances for a given m;

$$Z_m^\parallel(\omega) = \frac{\omega}{c} Z_m^\perp(\omega) \,.$$

11 Some analytical examples of impedances and wake functions

We mentioned earlier that there are three ways that wakefields are generated:

1. the beam is not relativistic;
2. the vacuum chamber is resistive;
3. the vacuum chamber is not smooth.

Three cases, each representing one of these three ways, that permit analytical expressions are given below.

11.1 Direct space charge

This wakefield and impedance come about when the beam is not sufficiently relativistic. Figure 10 shows the space charge wakefields in the x–y plane driven by an annular, infinitely thin, $\cos m\theta$ ring beam.

With a beam of radius a in a perfectly conducting round pipe of radius b and length L, we have the results of Table 2, where $Z_0 = \sqrt{\mu_0/\epsilon_0} \approx 377\ \Omega$. ($Z_0$ is the impedance of the vacuum. Yes, the vacuum has an impedance. An oscillating electromagnetic source will readily radiate into the vacuum,
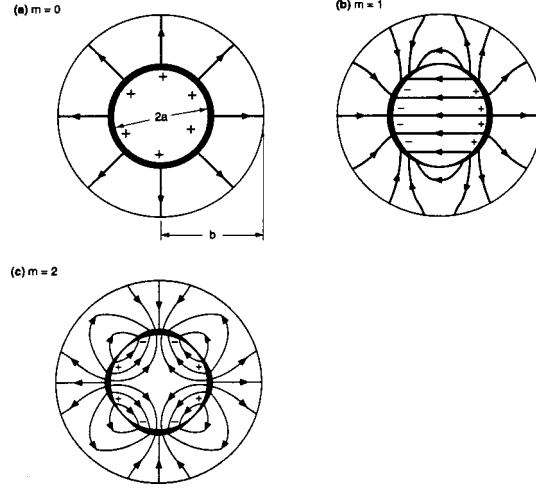
Fig. 10: Space charge wakefields in the x–y plane driven by an annular, infinitely thin, $\cos m\theta$ beam

Table 2: Results for direct space charge with a perfectly conducting vacuum chamber pipe

Impedances	Wake functions
$Z_0^{\parallel} = i\dfrac{Z_0 L \omega}{4\pi c \gamma^2}\left(1 + 2\ln\dfrac{b}{a}\right)$	$W_0' = \dfrac{Z_0 cL}{4\pi\gamma^2}\left(1 + 2\ln\dfrac{b}{a}\right)\delta'(z)$
$Z_{m\neq0}^{\perp} = i\dfrac{Z_0 L}{2\pi\gamma^2 m}\left(\dfrac{1}{a^{2m}} - \dfrac{1}{b^{2m}}\right)$	$W_{m\neq0} = \dfrac{Z_0 cL}{2\pi\gamma^2 m}\left(\dfrac{1}{a^{2m}} - \dfrac{1}{b^{2m}}\right)\delta(z)$

Table 3: Results for resistive wall

Impedances	Wake functions
$Z_m^{\parallel} = \dfrac{\omega}{c}Z_m^{\perp}$	$W_m = -\left(\dfrac{c}{\pi b^{m+1}(1 + \delta_{m0})}\right)\left(\sqrt{\dfrac{Z_0}{\pi\sigma_c}}\right)\left(\dfrac{L}{|z|^{1/2}}\right)$
$Z_m^{\parallel} = \left(\dfrac{1 - \text{sgn}(\omega)i}{1 + \delta_{0m}}\right)\left(\dfrac{L}{\pi\sigma_c\delta_{\text{skin}}b^{2m+1}}\right)$	$W_m' = -\left(\dfrac{c}{2\pi b^{m+1}(1 + \delta_{m0})}\right)\left(\sqrt{\dfrac{Z_0}{\pi\sigma_c}}\right)\left(\dfrac{L}{|z|^{3/2}}\right)$

thus losing energy. In fact, the vacuum impedance is very large. A well designed accelerator will have an impedance only a fraction of the vacuum impedance. Accelerators are very poor radiators compared with the vacuum, and this is done purposedly.)

Owing to the factor $1/\gamma^2$, space charge effects are most significant for low-to-medium energy proton or heavy-ion accelerators.

The space charge impedance is purely imaginary, and is $\propto i\omega$, as if it is a pure inductance. However, its sign is as if it is a capacitance. By convention, we call it 'capacitive'.

11.2 Resistive wall

Another case solvable analytically is for a round resistive pipe with radius b, conductivity σ_c, and length L. Defining the skin depth

$$\delta_{\text{skin}} = \sqrt{\frac{2c}{|\omega|Z_0\sigma_c}},$$

(For example, $\delta_{\text{skin}}\,[\text{mm}] = \dfrac{0.066}{\sqrt{f\,[\text{MHz}]}}$ for copper.) one finds the results of Table 3.
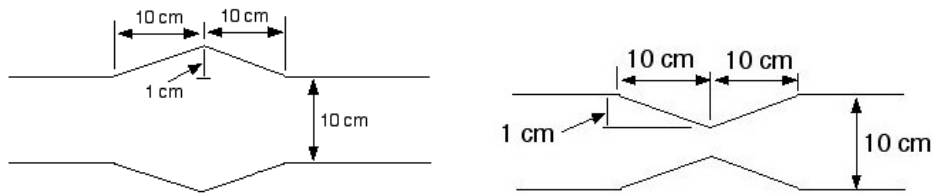
Fig. 11: Homework: find the impedances of these vacuum chamber geometries

The impedance is proportional to $(1 - \mathrm{i})$, i.e., it is half resistive and half inductive.

The $|z|^{-1/2}$ dependence of $W_m(z)$ indicates that the resistive wall wakefield (particularly, its transverse component) decays slowly and typically lasts long after the beam passage, sometimes long enough for the beam to see its own wakefield at its next revolution. The initial quick transient wakefields have been dropped in these expressions.

11.3 Slowly varying wall boundaries

The third way to generate impedances is by discontinuities. Consider a case when the vacuum chamber (perfectly conducting) wall varies along the accelerator slowly; a perturbation technique can be applied. Specify the wall variation by $h(z)$ (cylindrically symmetric bump). At low frequencies, $k = \omega/c < 1/(\text{bump length or depth})$. The impedance is purely inductive—opposite in sign to the space charge impedance,

$$Z_0^{\parallel} = -\frac{2\mathrm{i}kZ_0}{b} \int_0^{\infty} \kappa |\tilde{h}(\kappa)|^2 \mathrm{d}\kappa \,,$$

where

$$\tilde{h}(k) = \frac{1}{2\pi} \int_{-\infty}^{\infty} h(z) \mathrm{e}^{-\mathrm{i}kz} \mathrm{d}z \,.$$

When the boundary varies rapidly, this formula breaks down. Numerical calculation then has to be applied.

Homework

Find the impedances of the vacuum chamber geometries in Fig. 11.

12 Beam energy spread in a linac

Consider a beam bunch travelling down an accelerator along the axis of the vacuum chamber pipe. The $m = 0$ wakefield excited by the beam produces a longitudinal force on particles in the beam. The main effect of this longitudinal force is a retarding voltage, causing energy changes of individual particles. As a result, there is a net energy loss of the beam to the wakefields. Furthermore, since not all particles in the bunch lose the same amount of energy, the wakefield also causes the beam to acquire an energy *spread*.

12.1 One-particle model

Consider first a one-particle model in which the beam bunch is a macroparticle of charge Ne. Travelling down the linac, it experiences the self-generated retarding longitudinal field and loses energy

$$\Delta E = -\frac{1}{2}Ne^2 W_0'(0^-) \,,$$

where the factor $\frac{1}{2}$ is due to the fundamental theorem of beam loading.

Take the SLAC linac for example: $W_0'(0^-) = 7 \text{ cm}^{-1} \times (L_0/L)$, where L_0 is the total linac length, 3 km and L is the length of an RF structure cell, 3.5 cm. We find $\Delta E = 2.2$ GeV for $N = 5 \times 10^{10}$. (To convert cgs units to other units, one may apply $\frac{e^2}{mc^2} = r_0$, the classical radius of the particle under consideration.)

12.2 Two-particle model

This estimate can be improved by a two-particle model. The beam bunch is represented by two macro-particles, one leading and another trailing at a distance $|z|$. The parasitic loss per particle in the leading macroparticle due to its self-field is 1.1 GeV. The trailing macroparticle loses, in addition to the 1.1 GeV due to the self-field,

$$\Delta E = -\frac{1}{2}Ne^2W_0'(z) \,,$$

due to the wakefield left behind by the leading macroparticle.

Take $z = -\sigma_z = -1$ mm, $N = 5 \times 10^{10}$, and $W_0'(-1 \text{ mm}) = 4.5 \text{ cm}^{-1} \times (L_0/L)$, each particle in the trailing macroparticle loses an additional 1.4 GeV. The net loss of a trailing particle is 2.5 GeV.

The one-particle model estimates a parasitic loss per particle of 2.2 GeV. The two-particle model estimates an average loss of $(1.1 + 2.5)/2 = 1.8$ GeV. The two-particle model has introduced an energy split of 1.4 GeV, or a 2.8% energy spread if the beam energy at the end of the linac is 50 GeV.

12.3 An issue with linear colliders

For linear colliders, this energy spread makes it difficult to focus the beam to a small spot at the collision point in a final focus system, and is to be avoided. Most of this spread can be removed by properly phasing the accelerating RF voltage relative to the beam.

One concern for a high-intensity linear collider can be described as follows. The energy spread at the end of the linac scales is

$$\frac{\Delta E}{E} \approx \frac{\frac{1}{2}Ne^2W_0'}{GL_0} \approx \frac{\frac{1}{2}Ne^2}{Gb^2} \,,$$

where G is the acceleration gradient, and $W_0' \approx L_0/b^2$ is the longitudinal wake function, where b is the vacuum chamber radius characterizing the size of the accelerating cavities.

On the other hand, the efficiency of energy extraction by the beam from the field energy U stored in the accelerating cavities

$$U \approx \frac{1}{8\pi}\left(\frac{G}{e}\right)^2 \pi b^2 L_0$$

is given by

$$\text{extraction efficiency} \approx \frac{NE}{U} \approx \frac{8Ne^2}{Gb^2} \,,$$

which is found to be equal to 16 times the energy spread.

In other words, to improve the energy spread of the beam at the end of the linac necessitates sacrificing the energy extraction efficiency. One way to ameliorate this problem is to compensate $(\Delta E/E)$ by phasing the RF voltage. Another way is to send a *train* of M bunches per filling of the RF cavities. This will increase the energy extraction efficiency by a factor of M, although at the cost of having to deal with multibunch interactions due to the long-range wakefields.

12.4 General bunch distribution

We now depart from the simplified models and consider a bunch with a general longitudinal distribution $\rho(z)$. The energy change for a test charge e at longitudinal position z can be written as $eV(z)$, where

$$V(z) = -\int\limits_{z}^{\infty} \mathrm{d}z' \rho(z') W_0'(z - z')$$

or, equivalently,

$$V(z) = -\frac{1}{2\pi} \int\limits_{-\infty}^{\infty} \mathrm{d}\omega \, \mathrm{e}^{\mathrm{i}\omega z/c} Z_0^{\|}(\omega) \tilde{\rho}(\omega) \;.$$

A negative value of $V(z)$ means that the test charge loses energy from the wakefield. An additional integration of $V(z)$ over the bunch then gives the total parasitic loss,

$$\Delta\mathcal{E} = \int\limits_{-\infty}^{\infty} \rho(z) V(z) \mathrm{d}z \;.$$

For a bunch with Gaussian longitudinal distribution and uniform disc transverse distribution, for example, the energy spread due to space charge effects is

$$\frac{V(z)}{L} = \sqrt{\frac{2}{\pi}} \frac{q}{\gamma^2 \sigma_z^2} \left(\ln \frac{b}{a} + \frac{1}{2} \right) f\left(\frac{z}{\sigma_z} \right) \;,$$
$$f(u) = u \mathrm{e}^{-u^2/2} \;.$$

Generally, particles in the front of the bunch ($z > 0$) lose energy due to wakefields, while particles in the back of the bunch ($z < 0$) may gain or lose energy, depending on the length of the bunch. This is not true for the special case of the space charge effect, for which particles in the front of the bunch gain energy, and particles in the back of the bunch lose energy. For the space charge effect, the energy gained by the bunch head is necessarily given up by the bunch tail so that the net energy of the bunch is unchanged.

Consider a numerical example of a 50 MeV proton transport line. If we take $q = 10^{10} e$, $\sigma_z = 3$ cm, $a = 2$ cm, and $b = 5$ cm, we obtain a longitudinal space charge force of ± 6 V/m for particles located at $z = \pm\sigma_z$. The net energy change of these particles after travelling 100 m of this transport line is $eV/\beta = \pm 2$ keV. The space charge induced beam energy spread is therefore $\pm 4 \times 10^{-5}$.

For a resistive wall, we have

$$\frac{V(z)}{L} = \frac{q}{4b\sigma_z^{3/2}} \sqrt{\frac{c}{2\pi\sigma}} f\left(\frac{z}{\sigma_z} \right) \;,$$
$$f(u) = -|u|^{3/2} \mathrm{e}^{-u^2/4} \left[(I_{-1/4} - I_{3/4}) \operatorname{sgn}(u) - I_{1/4} + I_{-3/4} \right] \;,$$

with the Bessel functions $I_{\pm 1/4}$ and $I_{\pm 3/4}$ evaluated at $u^2/4$. Continuing this numerical example, assuming an aluminium pipe, a particle located at $0.5\sigma_z$ ahead of the bunch centre loses an energy of 0.1 eV after travelling 100 m, and a particle located at $1.8\sigma_z$ behind the bunch centre gains 0.04 eV.

13 Beam break-up in a linac

In the previous section, the beam was centred in a cylindrically symmetric pipe. There were no transverse wake forces ($m = 0$). If the beam is executing a betatron oscillation, an $m = 1$ dipole wakefield is excited by the bunch head, which causes transverse deflection of the bunch tail. For a high-intensity beam, this leads to a transverse break-up of the beam. The first observation of beam break-up was made on the SLAC linac.
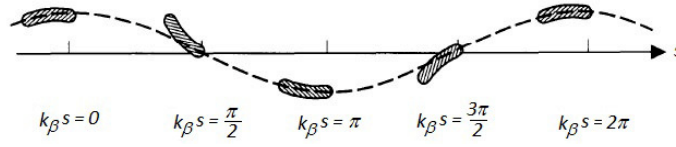
Fig. 12: Propagation of beam along linac

13.1 Two-particle model

To proceed with a simplified macroparticle model, we first note that a one-particle model is not useful because a point charge does not exert a transverse wake force on itself. In the two-particle model, the leading macroparticle, unperturbed by its own transverse wakefield, executes a free betatron oscillation

$$y_1(s) = \hat{y} \cos k_\beta s .$$

The trailing macroparticle, at a distance $|z|$, sees a deflecting wakefield left behind by its leading partner,

$$
\begin{aligned}
y_2'' + k_\beta^2 y_2 &= -\frac{Ne^2 W_1(z)}{2EL} y_1 \\
&= -\frac{N r_0 W_1(z)}{2\gamma L} \hat{y} \cos k_\beta s ,
\end{aligned}
$$

where $W_1(z)$ is the transverse wake function per cavity period L. We have ignored acceleration of the beam energy. For the SLAC linac, $k_\beta \approx 0.06 \text{ m}^{-1}$ and $k_\beta L \approx 0.002$.

The solution is

$$y_2(s) = \hat{y}\left[\cos k_\beta s - \frac{N r_0 W_1(z)}{4 k_\beta \gamma L} s \sin k_\beta s\right] .$$

The first term describes the free oscillation and the second term is the resonant response to the driving wake force. The amplitude of the second term grows linearly with s. The mechanism of the beam break-up is that particles in the tail of the beam are driven exactly on resonance by the oscillating wake left by the head of the beam.

At the end of the linac, the oscillation amplitude of the bunch tail relative to the bunch head is characterized by the dimensionless growth parameter

$$\Upsilon = -\frac{N r_0 W_1(z) L_0}{4 k_\beta \gamma L} ,$$

where L_0 is the total linac length.

For a beam bunch with realistic distribution, the bunch is distorted into a banana shape. The motion of the bunch head is $\cos k_\beta s$, while the deviation of the bunch tail relative to the bunch head is $s \sin k_\beta s$. When the bunch head is at a maximum displacement, the tail lines up with the bunch head, but when the bunch head displacement is zero, the tail swing is maximum (Fig. 12). As the beam propagates down the linac, the swing amplitude of the flapping tail increases with s until the tail breaks up and particles are lost. Note that the sign of the tail swing shown is not arbitrary, because $\Upsilon > 0$.

Figure 13 shows four transverse beam profiles observed at the end of the SLAC linac with $N = 2 \times 10^{10}$. The leftmost profile is for a carefully steered beam. When the beam was injected off centre by 0.2, 0.5, and 1 mm, the beam profiles were as shown in the corresponding right-hand panels. The beam sizes σ_x and σ_y were $\sim$120 µm.
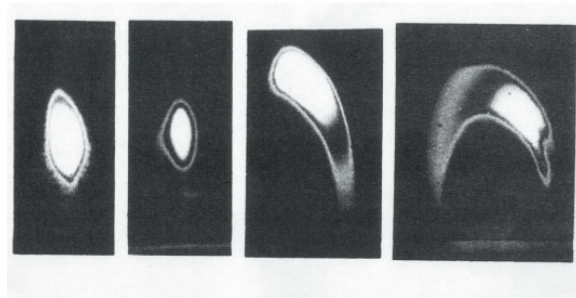
Fig. 13: Four transverse beam profiles observed at the end of the SLAC linac with $N = 2 \times 10^{10}$. From left to right: beam centred, beam offset by 0.2, 0.5, and 1 mm, respectively. (Courtesy John Seeman)

13.2 With acceleration

So far we have ignored beam acceleration, which has an important stabilizing effect because, as its energy increases, the beam becomes more rigid and less vulnerable to the wakefields. Furthermore, the driving beam's displacement also decreases with adiabadic damping. Repeating a similar analysis but taking acceleration into account yields the growth parameter

$$ \Upsilon = -\frac{N r_0 W_1(z) L_0}{4 k_\beta \gamma_f L} \ln \frac{\gamma_f}{\gamma_i} \, , $$

which is basically simply replacing the factor L_0/γ with its integral counterpart $\int_0^{L_0} \mathrm{d}s/\gamma(s)$. Owing to acceleration, the tail amplitude thus grows logarithmically rather than linearly with s, and the growth parameter is much reduced. If the beam is accelerated in the SLAC linac from 1 to 50 GeV, the factor Υ becomes 14, instead of 180 if the beam coasts at 1 GeV.

The beam break-up instability described so far is quite severe, even with acceleration. To control it, the beam has to be tightly focused, rapidly accelerated, and carefully injected, and its trajectory must be carefully steered down the linac. Interestingly, the contribution from trajectory mis-steering can, in principle, be largely compensated for by an intentional mis-injection.

13.3 BNS damping

It turns out, however, that there is another interesting and effective method to ameliorate the situation. This method, known as *BNS damping*, after Balakin, Novokhatsky, and Smirnov, is described next.

Consider first the case without acceleration, where the leading macroparticle executes a free betatron oscillation. The idea of BNS damping requires the introduction of a slightly stronger betatron focusing of the bunch tail than the bunch head. The equation of motion of the tail particles can be written as

$$ y_2'' + (k_\beta + \Delta k_\beta)^2 y_2 = -\frac{N r_0 W_1(z)}{2 \gamma L} \hat{y} \cos k_\beta s \, . $$

The solution, assuming $|\Delta k_\beta / k_\beta| \ll 1$, is

$$ y_2(s) = \hat{y} \cos(k_\beta + \Delta k_\beta)s + \frac{N r_0 W_1(z)}{4 k_\beta \Delta k_\beta \gamma L} \hat{y} \big[\cos(k_\beta s + \Delta k_\beta s) - \cos k_\beta s \big] \, . $$

Compared with the result without Δk_β, one observes that, by introducing a slightly different focusing strength for the bunch tail, the beam break-up mechanism of the bunch head resonantly driving the bunch tail is removed. A further inspection shows that there exists a magical condition for the bunch tail to follow the bunch head exactly for all s, namely

$$ \frac{N r_0 W_1(z)}{4 k_\beta \Delta k_\beta \gamma L} = -1 \, , $$

or, equivalently,

$$\frac{\Delta k_\beta}{k_\beta} = -\frac{N r_0 W_1(z)}{4 k_\beta^2 \gamma L} = \frac{\Upsilon}{k_\beta L_0} \,, \tag{6}$$

where Υ is as defined before, and $k_\beta L_0$ is the total betatron phase advance of the linac. For short bunches, Υ and Δk_β are positive; the betatron focusing required to fulfil the BNS condition is therefore stronger at the bunch tail than at the bunch head.

Under the BNS condition, $y_2(s) = y_1(s) = \hat{y} \cos k_\beta s$, and the beam no longer breaks up. (The mechanism of BNS damping is not to be confused with that of Landau damping, to be discussed later. They have little in common other than the fact that both involve a frequency spread in the bunch population.) Physically, this happens because the additional external focusing force introduced for the bunch tail has compensated for the defocusing dipole deflection force due to the wakefield left behind by the bunch head. Note that the BNS focusing has to be adjusted according to the beam intensity.

There are different ways to provide the BNS focusing. One is to introduce a radio-frequency quadrupole whose strength changes as the bunch passes by, so that the head and tail of the bunch see different quadrupole strengths. Another is to choose the location of the bunch relative to the acceleration RF voltage in such a way that the bunch tail acquires a lower energy than the bunch head. The energy spread across the bunch then causes a spread in betatron focusing according to

$$\frac{\Delta k_\beta}{k_\beta} = \xi \frac{\Delta E}{E} \,,$$

where ξ is the chromaticity determined by the linac design. For a FoDo lattice design, for example,

$$\xi = -\frac{2}{\mu} \tan \frac{\mu}{2} \,,$$

where μ is the betatron phase advance per FoDo cell. By properly choosing the phase of the RF voltage relative to the beam bunch, the betatron focusing required by the BNS condition can be obtained, provided the required $\Delta k_\beta / k_\beta$ is not excessive.

For an accelerated beam, the BNS condition is still given by Eq. (6), except that the parameter Υ is now that given by the case with acceleration. Take the SLAC linac, for example, and assume $\mu = 90°$; then the energy deviation of the bunch tail from the bunch head required by the BNS condition is about -5.5%. BNS damping has been routinely employed to control the beam break-up instability in the SLAC linac operations.

14 Parasitic heating

When a beam bunch of charge q and line density $\lambda(t)$ traverses an impedance $Z_0^\parallel(\omega)$, it loses energy to the impedance. This *parasitic energy loss* (or higher-order mode heating) is

$$\Delta \mathcal{E} = -\kappa^\parallel q^2 \,,$$

where $\kappa^\parallel$ is the *loss factor*, in units of V/pC,

$$\kappa^\parallel = \frac{1}{\pi} \int_0^\infty d\omega \, \mathrm{Re} \, Z_0^\parallel(\omega) \, |\tilde{\lambda}(\omega)|^2 \,. \tag{7}$$

For a Gaussian bunch, $\lambda(t) = e^{-t^2/2\sigma^2}/(\sqrt{2\pi}\sigma)$, $\tilde{\lambda}(\omega) = e^{-\omega^2\sigma^2/2}$.

Only the real part of the impedance contributes to the parasitic loss. The space charge or the slowly varying wall impedances do not cause net energy loss to the beam. However, this does not mean that individual particles do not change their energies. It only means that there is energy transfer among different parts of the bunch, while the total energy of the whole bunch remains unchanged.

For a resistive wall,

$$\frac{\kappa^{\|}(\sigma)}{L} = \frac{\Gamma(\frac{3}{4})c}{4\pi^2 b \sigma_z^{3/2}} \left(\frac{Z_0}{2\sigma_c}\right)^{1/2}, \qquad \Gamma\left(\frac{3}{4}\right) = 1.225 .$$

where b is the pipe radius (assumed cylindrically symmetrical). It shows explicitly that parasitic loss is more pronounced for short bunches.

Parasitic loss gives rise to heating of the vacuum chamber wall where there are impedances. In high-intensity electron storage rings, the beam position monitors or bellows can heat up. This is especially serious for short bunches.

Most of the parasitic loss occurs as the beam traverses a discontinuity structure. Part of the wakefield gets trapped if the structure is cavity-like and if the wakefield frequency is below the cut-off frequency of the pipe. The trapped field energy is eventually deposited as heat on the cavity walls. The rest of the wakefield, with frequency higher than the cut-off frequency, propagates up and down the pipe and eventually dissipates on lossy material elsewhere in the vacuum chamber. For a cavity structure, $\kappa^{\|}$ is given by a sum over cavity modes below the cut-off frequency, plus a contribution above the cut-off frequency. Each cavity mode below the cut-off frequency contributes a resonator impedance, with

$$\kappa^{\|} \approx \begin{cases} \dfrac{\omega_r R_{\rm s}}{2Q_r} e^{-\omega_r^2 \sigma^2} & \text{high-}Q \text{ resonator}, \\[2ex] \dfrac{\omega_r R_{\rm s}}{2Q_r} & \text{low-}Q \text{ resonator, short bunch } \omega_r\sigma \ll 1, \\[2ex] \dfrac{R_{\rm s}}{4\sqrt{\pi}Q_r^2\omega_r^2\sigma^3} & \text{low-}Q \text{ resonator, long bunch } \omega_r\sigma \gg 1 . \end{cases}$$

Above the cut-off frequency, the impedance per cavity can be represented by the diffraction model,

$$Z_0^{\|}(\omega) = [1 + \text{sgn}(\omega)\text{i}]\frac{Z_0}{2\pi^{3/2}}\frac{1}{b}\sqrt{\frac{cg}{|\omega|}} ,$$

where g is the gap size of the cavity. This impedance has both real and imaginary parts.

For a single bunch in a circular accelerator, the integral in Eq. (7) is replaced by an infinite sum,

$$\kappa^{\|}(\sigma) = \frac{\omega_0}{2\pi} \sum_{p=-\infty}^{\infty} Z_0^{\|}(p\omega_0) \, |\tilde{\lambda}(p\omega_0)|^2 .$$

For short bunches in large accelerators ($\omega_0 \ll 1/\sigma$), the sum can be replaced by an integral, and the difference between single passes and multiple passes disappears.

The parasitic loss by the beam goes into wakefields. Typically, only a small fraction of the particle energy becomes wakefields; most of the energy stored in the wakefields ends up as heat on the vacuum chamber walls. However, under unfavourable conditions, a small portion of the wakefield energy can be transferred systematically back to beam motion, causing beam instabilities. Parasitic loss, therefore, is the ultimate culprit for the various collective instabilities.

15 The Vlasov equation

The Vlasov equation describes the collective behaviour of a multiparticle system under the influence of electromagnetic forces. To construct the Vlasov equation, one starts with the single-particle equations of motion (assume 1D):

$$\begin{aligned} \dot{q} &= f(q,p,t) \\ \dot{p} &= g(q,p,t) . \end{aligned}$$
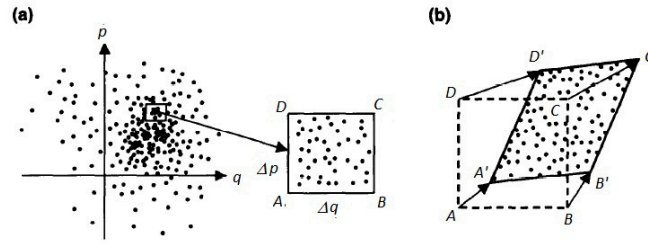
Fig. 14: Derivation of the Vlasov equation

The state of a particle at a given time t is represented by a point in the phase space (q, p). The motion of a particle is described by the motion of its representative point in phase space.

In a conservative deterministic system, the particle trajectory in phase space is completely determined by the initial conditions (q_0, p_0) at time $t = t_0$. Two particles having the same initial conditions must have exactly the same trajectory in phase space. It follows that the only way for two trajectories to meet at a given time is for them to coincide at all times. In other words, trajectories either completely coincide or never intersect.

Consider a distribution of particles occupying an area in the phase space. Because they cannot intersect with particles on the boundary of the distribution as the distribution evolves in time, particles inside cannot leak out of and particles outside cannot enter the distribution.

If the system is conservative,

$$f = \frac{\partial H}{\partial p} \quad \text{and} \quad g = -\frac{\partial H}{\partial q} \, ,$$

where H is the Hamiltonian. It follows that

$$\frac{\partial f}{\partial q} + \frac{\partial g}{\partial p} = 0 \, .$$

As will be seen later, this condition leads to an area preservation property: as the particle distribution evolves in the phase space, its shape may be distorted but its area remains constant. In fact, in a non-conservative system, $\frac{\partial f}{\partial q} + \frac{\partial g}{\partial p}$ has the physical meaning of the rate of area shrinkage.

Consider a distribution of a group of particles in phase space at time t. A rectangular $\Delta q \, \Delta p$ box is drawn (Fig. 14(a)):

$$A(q, \, p) \, ,$$
$$B(q + \Delta q, \, p) \, ,$$
$$C(q + \Delta q, \, p + \Delta p) \, ,$$
$$D(q, \, p + \Delta p) \, .$$

At a later time, $t + \mathrm{d}t$, the box moves and deforms into a parallelogram $A'B'C'D'$ (Fig. 14(b)) with the same area as $ABCD$. All particles inside the box move with the box. Let the number of particles enclosed by the box be

$$\psi(q, p, t) \, \Delta q \, \Delta p \, ,$$

where ψ is the phase space distribution density normalized by

$$\int\limits_{-\infty}^{\infty} \mathrm{d}q \int\limits_{-\infty}^{\infty} \mathrm{d}p \, \psi(q, p, t) = N \, .$$

61

The vertices of the parallelogram are

$$A'[q + f(q,p,t)\mathrm{d}t,\ p + g(q,p,t)\mathrm{d}t]\ ,$$
$$B'[q + \Delta q + f(q + \Delta q, p, t)\mathrm{d}t,\ p + g(q + \Delta q, p, t)\mathrm{d}t]\ ,$$
$$C'[q + \Delta q + f(q + \Delta q, p + \Delta p, t)\mathrm{d}t,\ p + \Delta p + g(q + \Delta q, p + \Delta p, t)\mathrm{d}t]\ ,$$
$$D'[q + f(q, p + \Delta p, t)\mathrm{d}t,\ p + \Delta p + g(q, p + \Delta p, t)\mathrm{d}t]\ .$$

The condition that no particles leak into or out of the box gives

$$\psi(q,\ p,\ t)\ \mathrm{area}(ABCD) = \psi(q + f\mathrm{d}t,\ p + g\mathrm{d}t,\ t + \mathrm{d}t)\ \mathrm{area}(A'B'C'D')\ .$$

For a Hamiltonian system, the area of the box is conserved:

$$\mathrm{area}(A'B'C'D') = |\overrightarrow{A'B'} \times \overrightarrow{A'D'}|$$

$$= \Delta q\,\Delta p \left[1 + \left(\frac{\partial f}{\partial q} + \frac{\partial g}{\partial p} \right) \mathrm{d}t \right]$$

$$= \Delta q\,\Delta p = \mathrm{area}(ABCD)\ .$$

We then have

$$\psi(q,p,t) = \psi(q + f\mathrm{d}t,\ p + g\mathrm{d}t,\ t + \mathrm{d}t)$$

$$= \psi + \frac{\partial \psi}{\partial q} f\mathrm{d}t + \frac{\partial \psi}{\partial p} g\mathrm{d}t + \frac{\partial \psi}{\partial t}\mathrm{d}t\ ,$$

or, after cancelling out ψ on both sides, we obtain the *Vlasov equation*

$$\frac{\partial \psi}{\partial t} + f\frac{\partial \psi}{\partial q} + g\frac{\partial \psi}{\partial p} = 0\ .$$

The Vlasov equation can also be put in a much more vague form:

$$\frac{\mathrm{d}\psi}{\mathrm{d}t} = 0, \quad \text{or} \quad \psi = \text{constant in time.}$$

Sometimes loosely referred to as the *Liouville theorem*, this form states that the local particle density does not change if (an important if) the observer moves with the flow of boxes, but it does not tell how the boxes flow. The Vlasov form, in contrast, does not have this ambiguity, since it explicitly contains the single-particle information f and g.

Strictly speaking, f and g are given by external forces. Collisions among discrete particles in the system, for example, are excluded. However, if a particle interacts more strongly with the *collective* fields of the other particles than with its nearest neighbours, the Vlasov equation still applies if one treats the collective fields on the same footing as the external fields. In fact, this forms the basis of treating the collective instabilities using the Vlasov technique.

One special case where the Vlasov equation can be solved exactly is when the system is described by a Hamiltonian $H(q,p)$ that does not have an explicit time dependence. A stationary solution is found to be

$$\psi(q,p) = \text{any function of } H(q,p)\ .$$

In this system, individual particles stream along constant-H contours in phase space in such a way that the overall distribution is stationary.

In the derivation of the Vlasov equation, we have assumed that there are no diffusion or external damping effects. This is usually a good approximation for proton beams. For electron beams, synchrotron radiation contributes to both damping and diffusion, and one needs to apply the *Fokker–Planck equation*, a generalization of the Vlasov equation. However, when the instability occurs faster than the damping or diffusion times, the Vlasov treatment also at least approximately applies to electrons.

16 Potential-well distortion

As a first application of the Vlasov technique, we study the effect of a longitudinal wakefield on a distortion of the equilibrium shape of a beam bunch. The mechanism is a static one; no part of the beam bunch is executing collective oscillation. The extent of distortion depends on the beam intensity; higher beam intensities cause larger distortions.

Consider a bunched beam that travels along the axis of the vacuum chamber pipe in a circular accelerator. We assume that the beam does not have any transverse dimension, i.e., the beam is an infinitesimally thin thread. Such a beam does not generate transverse wakefields; only the $m = 0$ wake is excited.

Consider a particle in the beam executing longitudinal synchrotron oscillation. The phase space coordinates q and p are

$$q = z \quad \text{and} \quad p = -\frac{\eta c}{\omega_\text{s}}\delta \,,$$

where η is the slippage factor defined by the accelerator lattice and ω_s is the synchrotron oscillation frequency.

The single-particle equations of motion are

$$z' = -\eta\delta \quad \text{and} \quad \delta' = K(z) \,.$$

We leave $K(z)$ open for now, except that we do know it cannot depend on δ, because the system is conservative.

The Vlasov equation reads

$$\frac{\partial\psi}{\partial s} - \eta\delta\frac{\partial\psi}{\partial z} + K(z)\frac{\partial\psi}{\partial\delta} = 0 \,,$$

where we will set $\partial\psi/\partial s = 0$, since we are looking for a stationary distribution. The general stationary solution is

$$\psi(z,\delta) = \text{any function of the Hamiltonian } H \,,$$
$$H = \frac{\eta^2 c^2}{\omega_\text{s}}\left[\frac{\delta^2}{2} + \frac{1}{\eta}\int_0^z K(z')\mathrm{d}z'\right] \,.$$

The second integral term in H is the potential-well term. A simple harmonic system would have a parabolic potential well.

If the potential well is provided by an external RF voltage $V_\text{RF}(z)$, we have

$$K(z) = \frac{eV_\text{RF}(z)}{CE} = \frac{\omega_\text{s}^2}{c^2\eta V_\text{RF}'(0)}V_\text{RF}(z) \,.$$

A practical case is given by $V_\text{RF} = \hat{V}\sin(\omega_\text{RF}z/c)$. The deviation of $V_\text{RF}(z)$ from a linear dependence on z is a cause of potential-well distortion. The general stationary distribution is given by any function of the Hamiltonian

$$H = \frac{\eta^2 c^2}{2\omega_\text{s}}\delta^2 + \frac{\omega_\text{s}c^2}{\omega_\text{RF}^2}\left[1 - \cos\left(\frac{\omega_\text{RF}z}{c}\right)\right] \,.$$

This Hamiltonian also describes the form of the RF bucket. A stationary distribution must conform to the contours of constant Hamiltonian inside the bucket. For small oscillation amplitudes, we have $K = \omega_\text{s}^2 z/\eta c^2$, the case of simple harmonic motion.

One noteworthy special case of the stationary beam distribution is that given by $\exp(-\text{constant} \times H)$. This distribution is always Gaussian in δ. If the bunch length is much shorter than the RF wavelength, ($z \ll c/\omega_\text{RF}$) the familiar quadratic form of the Hamiltonian is re-established, and the distribution

is also Gaussian in z. As the bunch length increases, the bunch shape deviates from Gaussian; the potential well is distorted by the RF bucket, although the distribution remains Gaussian in δ.

There is another reason for the Hamiltonian to deviate from the quadratic form, and thus to cause potential-well distortion; namely, the wakefields. Consider a bunch that is short compared with the RF wavelength. Let the wake function be $W_0'(z)$ integrated over the accelerator circumference, and assume that the wake has dissipated before the beam completes one revolution,

$$K(z) = \frac{\omega_{\mathrm{s}}^2}{\eta c^2} z - \frac{r_0}{\gamma C} \int\limits_z^\infty \mathrm{d}z' \, \rho(z') W_0'(z - z') \, .$$

The corresponding Hamiltonian is

$$H = \frac{\eta^2 c^2}{2\omega_{\mathrm{s}}} \delta^2 + \frac{\omega_{\mathrm{s}}}{2} z^2 - \frac{\eta c^2 r_0}{\omega_{\mathrm{s}} \gamma C} \int\limits_0^z \mathrm{d}z'' \int\limits_{z''}^\infty \mathrm{d}z' \, \rho(z') W_0'(z'' - z') \, .$$

The stationary solution to the Vlasov equation must be a function of H. The complication here is that the complicated z-dependence of H now involves the beam density ρ, which in turn is determined by the stationary distribution itself. Clearly some self-consistency requirement is to be imposed.

Continuing the Gaussian example, the stationary distribution maintains its Gaussian distribution in δ,

$$\psi(z, \delta) = \frac{1}{\sqrt{2\pi}\sigma_\delta} \exp\left(-\frac{\delta^2}{2\sigma_\delta^2}\right) \rho(z) \, .$$

The Gaussian form and the value of σ_δ are arbitrary if the collective behaviour is governed by the Vlasov equation, as in the case of a proton beam. However, if the beam behaviour is governed, as for an electron beam, by the Fokker–Planck equation, then this Gaussian distribution with a specific value for σ_δ will be the unique solution of the stationary beam distribution.

This distribution matches the stationary solution

$$\psi(z, \delta) \propto \exp\left(-\frac{\omega_{\mathrm{s}}}{\eta^2 c^2 \sigma_\delta^2} H\right) \, .$$

Self-consistency then imposes a transcendental equation for $\rho(z)$, called the *Haissinski equation*,

$$\rho(z) = \rho(0) \exp\left[-\frac{1}{2}\left(\frac{\omega_{\mathrm{s}} z}{\eta c \sigma_\delta}\right)^2 + \frac{r_0}{\eta \sigma_\delta^2 \gamma C} \int\limits_0^z \mathrm{d}z'' \int\limits_{z''}^\infty \mathrm{d}z' \, \rho(z') W_0'(z'' - z')\right] \, .$$

In the limit of zero beam intensity, the solution reduces to the bi-Gaussian form, where $\sigma_z = \eta c \sigma_\delta / \omega_{\mathrm{s}}$. For high beam intensities, $\rho(z)$ deforms from a Gaussian. The Haissinski equation is solved numerically for $\rho(z)$ once $W_0'(z)$ is known and σ_δ is specified. Figure 15 shows the result for the electron damping ring for the SLAC Linear Collider. The bunch shape is Gaussian at low beam intensities, and distorts as the beam intensity is increased. The calculations agree with the measurements.

Note that the distribution leans forward ($z > 0$) as the beam intensity increases. This effect comes from the parasitic loss of the beam bunch, and is a consequence of the real (resistive) part of the impedance. Since the SLAC damping ring is operated above transition, the bunch moves forward so that the parasitic energy loss can be compensated by the RF voltage.

Note also that the bunch length increases as the beam intensity increases. The bunch shape distortion comes mainly from the imaginary part of the impedance. That the bunch lengthens is a consequence of the fact that the imaginary part of the impedance is mostly inductive.
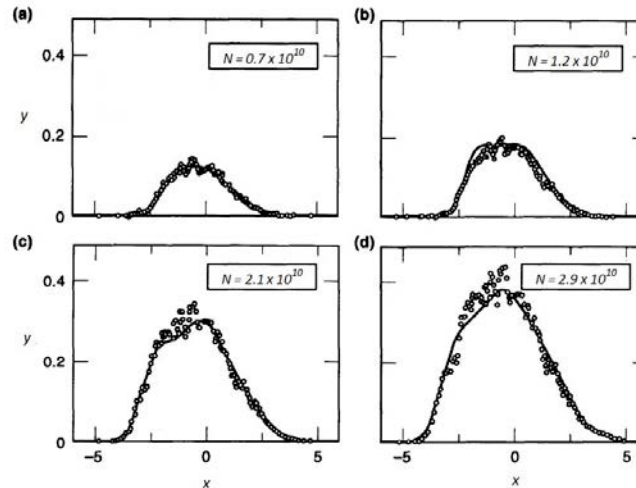
Fig. 15: Potential-well distortion for the electron damping ring for the SLAC Linear Collider. The bunch shape is Gaussian at low beam intensities and distorts as the beam intensity is increased. The horizontal axis is $x = -z/\sigma_{z0}$, where σ_{z0} is the unperturbed rms bunch length. The vertical scale gives $y = 4\pi e\rho(z)/V'_{\mathrm{RF}}(0)\sigma_{z0}$. (Courtesy Karl Bane, 1992.)

Fig. 16: Kenneth Robinson (1925–1979)

17   Robinson instability

The Robinson instability (named for Kenneth Robinson, Fig. 16) is one of the most basic instability mechanisms. It is a longitudinal instability that occurs in circular accelerators. The main contributor to this instability is the longitudinal impedance due to the RF accelerating cavities. These cavities are tuned to have a resonant frequency ω_{R} for its fundamental accelerating mode. This mode is what the klystrons feed into but, at the same time, it is also a big source of impedance. Since we must have this RF mode to accelerate the beam, we must accept its large impedance and live with it.

The real part of this impedance narrowly peaks at ω_{R}, the width $\Delta\omega/\omega_{\mathrm{R}} \approx \pm 1/Q$. Typically, $Q \sim 10^4$ (or 10^9 for superconducting cavities).

By design, ω_{R} is very close to an integer multiple of the revolution frequency ω_0. This necessarily means that the wakefield excited by the beam in the cavities contains a major frequency component near $\omega_{\mathrm{R}} \approx h\omega_0$, and the impedance $Z_0^{\|}(\omega)$ has sharp peaks at $\pm h\omega_0$, where h is an integer called the *harmonic number*.

As we will soon show, the exact value of ω_{R} relative to $h\omega_0$ is of critical importance for the

stability of the beam. Above transition, the beam will be unstable if ω_R is slightly above $h\omega_0$ and stable if slightly below. Below transition, it is the other way around.

Consider a one-particle model. The beam is just a big point charge Ne, without internal structures, and consider its longitudinal motion under the influence of its own longitudinal wakefield. Let z_n be the longitudinal displacement of the beam at the accelerating RF cavity in the nth revolution. The rate of change of z_n is related to the relative energy error δ_n of the beam in the same nth revolution by

$$\frac{\mathrm{d}}{\mathrm{d}n}z_n = -\eta C \delta_n \ .$$

The storage ring is above transition if $\eta > 0$ and below transition if $\eta < 0$.

The energy error also changes with time. In the absence of wakefields, its equation of motion is

$$\frac{\mathrm{d}}{\mathrm{d}n}\delta_n = \frac{(2\pi\nu_s)^2}{\eta C}z_n \ ,$$

where ν_s is the unperturbed synchrotron tune. If we combine these two equations, we get a simple harmonic oscillation for both z_n and δ_n, i.e., the normal synchrotron oscillation.

But for an intense beam, we have to add the wakefield term,

$$\begin{aligned}
\frac{\mathrm{d}}{\mathrm{d}n}\delta_n &= \frac{(2\pi\nu_s)^2}{\eta C}z_n + \frac{eV(z_n)}{E}\\
&= \frac{(2\pi\nu_s)^2}{\eta C}z_n - \frac{Nr_0}{\gamma}\sum_{k=-\infty}^{n}W_0'(kC - nC + z_n - z_k) \ ,
\end{aligned}$$

where W_0' is the longitudinal wake function accumulated over one turn of the accelerator. The summation over k is over the wakefields left behind by the beam from all revolutions prior to the nth. The equation of motion now becomes

$$\frac{\mathrm{d}^2 z_n}{\mathrm{d}n^2} + (2\pi\nu_s)^2 z_n = \frac{Nr_0\eta C}{\gamma}\sum_{k=-\infty}^{n}W_0'(kC - nC + z_n - z_k) \ .$$

If the beam bunch has an oscillation amplitude much shorter than the wavelength of the fundamental cavity mode, one can expand the wake function,

$$W_0'(kC - nC + z_n - z_k) \approx W_0'(kC - nC) + (z_n - z_k)W_0''(kC - nC) \ .$$

The first term is a static term independent of the motion of the beam. It describes the parasitic loss effect discussed earlier and can be taken care of by a constant shift in z_n. We will drop this term altogether because here we are interested only in the dynamical effects. The second term does involve the dynamics of the beam. The quantity $z_n - z_k$ is the difference of the z terms and – although we will not make such an approximation – resembles a time derivative $\mathrm{d}z/\mathrm{d}n$, which in turn suggests an instability, since a $\mathrm{d}z/\mathrm{d}n$ term in a $\mathrm{d}^2 z/\mathrm{d}n^2$ equation indicates a possible exponential growth (or damping) of z.

We now need to solve this equation for z_n as a function of n. To do so, let

$$z_n \propto \mathrm{e}^{-in\Omega T_0} \ ,$$

where Ω is the mode frequency of the beam oscillation and is a key quantity yet to be determined.

Substituting into the equation of motion, we find an algebraic equation for Ω,

$$\Omega^2 - \omega_s^2 = -\frac{Nr_0\eta c}{\gamma T_0}\sum_{k=-\infty}^{\infty}(1 - \mathrm{e}^{-ik\Omega T_0})W_0''(kC) \ ,$$

where $\omega_{\rm s} = \nu_{\rm s}\omega_0$ is the unperturbed synchrotron oscillation frequency. Now the wake function can be expressed in terms of the impedance by a Fourier transform,

$$\Omega^2 - \omega_{\rm s}^2 = -{\rm i}\,\frac{Nr_0\eta}{\gamma T_0^2}\sum_{p=-\infty}^{\infty}\left[p\omega_0 Z_0^{\parallel}(p\omega_0) - (p\omega_0 + \Omega)Z_0^{\parallel}(p\omega_0 + \Omega)\right].$$

Given the impedance, this equation can in principle be solved for Ω. Note that Ω appears on both sides of the equation. Here, however, we take a perturbative approach and assume that Ω does not deviate much from $\omega_{\rm s}$ for modest beam intensities. We thus replace Ω with $\omega_{\rm s}$ on the right-hand side of the equation. Quantity Ω is then easily solved.

In general, Ω is complex. The real part of Ω is the perturbed synchrotron oscillation frequency of the collective beam motion, and the imaginary part gives the growth rate (or damping rate if negative) of the motion. We then obtain a *mode frequency shift*,

$$\begin{aligned}\Delta\Omega &= {\rm Re}(\Omega - \omega_{\rm s}) \\ &= \frac{Nr_0\eta}{2\gamma T_0^2\omega_{\rm s}}\sum_{p=-\infty}^{\infty}\left[p\omega_0{\rm Im}Z_0^{\parallel}(p\omega_0) - (p\omega_0 + \omega_{\rm s}){\rm Im}Z_0^{\parallel}(p\omega_0 + \omega_{\rm s})\right.,\end{aligned}$$

and an *instability growth rate*,

$$\tau^{-1} = {\rm Im}(\Omega - \omega_{\rm s}) = \frac{Nr_0\eta}{2\gamma T_0^2\omega_{\rm s}}\sum_{p=-\infty}^{\infty}(p\omega_0 + \omega_{\rm s}){\rm Re}Z_0^{\parallel}(p\omega_0 + \omega_{\rm s}l).$$

The imaginary part of the impedance contributes to the collective frequency shift. The real part contributes to the instability growth rate. Note that when we measure the synchrotron frequency in an actual operation, what shows up in the beam spectrum is not $\omega_{\rm s}$, but Ω.

So far, our result holds for arbitrary impedance. We now consider the resonator impedance for the fundamental cavity mode. The only significant contributions to the growth rate come from two terms in the summation, namely $p = \pm h$, assuming that $\omega_{\rm R}/Q \ll \omega_0$,

$$\tau^{-1} \approx \frac{Nr_0\eta h\omega_0}{2\gamma T_0^2\omega_{\rm s}}\left[{\rm Re}Z_0^{\parallel}(h\omega_0 + \omega_{\rm s}) - {\rm Re}Z_0^{\parallel}(h\omega_0 - \omega_{\rm s})\right].$$

Beam stability requires $\tau^{-1} \leq 0$. That is, the real part of the impedance must be less at frequency $h\omega_0 + \omega_{\rm s}$ than at frequency $h\omega_0 - \omega_{\rm s}$ if $\eta > 0$, and the other way around if $\eta < 0$. This condition gives the Robinson stability criterion that, above transition, the resonant frequency $\omega_{\rm R}$ of the fundamental cavity mode should be slightly detuned downwards from an exact integral multiple of ω_0. Below transition, it should be the other way around, as sketched in Fig. 17.

Physically, the Robinson instability comes from the fact that the revolution frequency of an off-momentum beam is not given by ω_0 but by $\omega_0(1 - \eta\delta)$. To illustrate the physical origin, consider a beam executing synchrotron oscillation above transition. Owing to the energy error of the beam, the impedance samples the beam signal at a frequency slightly below $h\omega_0$ if $\delta > 0$, and slightly above $h\omega_0$ if $\delta < 0$. To damp this synchrotron oscillation, we need to let the beam lose energy when $\delta > 0$ and gain energy when $\delta < 0$. This can be achieved by having an impedance that decreases with increasing frequency in the neighbourhood of $h\omega_0$. The Robinson stability criterion then follows.

When $\tau^{-1} > 0$, the beam is unstable because any accidental small synchrotron oscillation would grow exponentially. When $\tau^{-1} < 0$, the Robinson mechanism leads to exponential damping of any synchrotron oscillations of the beam. Robinson damping (or antidamping) can be rather strong. When the Robinson criterion is met, the synchrotron oscillation of the beam is 'Robinson damped' and this damping will help stabilize the beam against similar instabilities due to other impedance sources.
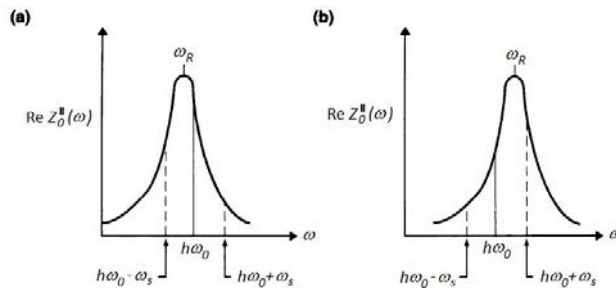
Fig. 17: Resonance frequency above and below transition

Table 4: Comparison of Robinson and strong head–tail instabilities

	Robinson instability	Strong head–tail instability
Dimension	Longitudinal	Transverse
Mode	$m = 0$	$m = 1$
Wakefield	Long-range	Short-range
Impedance	Sharply peaked	Broad-band
Model	One-particle	Two-particle
Threshold behaviour	No	Yes

18 Strong head–tail instability

We next introduce the strong head–tail instability, to be discussed using a two-macroparticle model. It was first observed and analysed at PEP. When the intensity exceeds a threshold, the beam becomes unstable. Below the threshold, the beam motion is perturbed but remains stable. Table 4 compares Robinson and strong head–tail instabilities.

The physical mechanism of the strong head–tail instability is closely related to beam break-up in linacs. Consider an idealized beam with two macroparticles, each with charge $Ne/2$ and each executing synchrotron oscillation. We assume that their synchrotron oscillations have equal amplitude but opposite phases. During time $0 < s/c < T_s/2$, where $T_s = 2\pi/\omega_s$ is the synchrotron oscillation period, particle 1 leads particle 2; the equations of motion are

$$
\begin{aligned}
y_1'' + \left(\frac{\omega_\beta}{c}\right)^2 y_1 &= 0 , \\
y_2'' + \left(\frac{\omega_\beta}{c}\right)^2 y_2 &= \frac{N r_0 W_0}{2\gamma C} y_1 ,
\end{aligned}
\tag{8}
$$

where ω_β is the unperturbed betatron oscillation frequency, whether horizontal or vertical. During $T_s/2 < s/c < T_s$, we have the same equations with indices 1 and 2 switched. Then during $T_s < s/c < 3T_s/2$, Eq. (8) applies again, etc.

In writing down Eq. (8), we have assumed for simplicity that the wake function (integrated over the accelerator circumference), $W_1(z)$, is a constant, and yet it vanishes before the beam completes one revolution,

$$
W_1(z) = \begin{cases} -W_0, & \text{if } 0 > z > -(\text{bunch length}) , \\ 0, & \text{otherwise} . \end{cases}
\tag{9}
$$

The property of wake functions requires that $W_0 > 0$. This short-range wake function corresponds to a broad-band impedance.

The solution for y_1 in Eq. (8) is simply a free betatron oscillation,

$$
\tilde{y}_1(s) = \tilde{y}_1(0) e^{-\mathrm{i}\omega_\beta s/c} ,
$$

68

where

$$\tilde{y}_1 = y_1 + \mathrm{i}\frac{c}{\omega_\beta}\, y_1' \, .$$

Substituting $\tilde{y}_1(s)$ into the equation for y_2 yields

$$\tilde{y}_2(s) = \tilde{y}_2(0)\mathrm{e}^{-\mathrm{i}\omega_\beta s/c} + \mathrm{i}\frac{Nr_0W_0c}{4\gamma C\omega_\beta}\left[\frac{c}{\omega_\beta}\tilde{y}_1^*(0)\sin\frac{\omega_\beta s}{c} + \tilde{y}_1(0)s\mathrm{e}^{-\mathrm{i}\omega_\beta s/c}\right] \, . \qquad (10)$$

The first two terms describe free betatron oscillation. The third term, proportional to s, is a resonantly driven response. This analysis is similar to the beam break-up instability.

Equation (10) can be simplified if $\omega_\beta \gg \omega_\mathrm{s}$. The second term can then be dropped. The solution during the period $0 < s/c < T_\mathrm{s}/2$ can be written in a matrix form,

$$\begin{bmatrix}\tilde{y}_1\\\tilde{y}_2\end{bmatrix}_{s=cT_\mathrm{s}/2} = \mathrm{e}^{-\mathrm{i}\omega_\beta T_\mathrm{s}/2}\begin{bmatrix}1 & 0\\\mathrm{i}\Upsilon & 1\end{bmatrix}\begin{bmatrix}\tilde{y}_1\\\tilde{y}_2\end{bmatrix}_{s=0} \, ,$$

with a positive, dimensionless parameter,

$$\Upsilon = \frac{\pi Nr_0W_0c^2}{4\gamma C\omega_\beta\omega_\mathrm{s}} \, .$$

The time evolution during $T_\mathrm{s}/2 < s/c < T_\mathrm{s}$ can be obtained by exchanging indices 1 and 2. The total transformation for one full synchrotron period is

$$\begin{bmatrix}\tilde{y}_1\\\tilde{y}_2\end{bmatrix}_{cT_\mathrm{s}} = \mathrm{e}^{-\mathrm{i}\omega_\beta T_\mathrm{s}}\begin{bmatrix}1 & \mathrm{i}\Upsilon\\0 & 1\end{bmatrix}\begin{bmatrix}1 & 0\\\mathrm{i}\Upsilon & 1\end{bmatrix}\begin{bmatrix}\tilde{y}_1\\\tilde{y}_2\end{bmatrix}_0$$

$$= \mathrm{e}^{-\mathrm{i}\omega_\beta T_\mathrm{s}}\begin{bmatrix}1-\Upsilon^2 & \mathrm{i}\Upsilon\\\mathrm{i}\Upsilon & 1\end{bmatrix}\begin{bmatrix}\tilde{y}_1\\\tilde{y}_2\end{bmatrix}_0 \, .$$

As time evolves, the phasors $\tilde{y}_1$ and $\tilde{y}_2$ are repeatedly transformed by the 2×2 matrix of this map. The stability of the system is determined by the eigenvalues of this matrix. The two eigenvalues (a $+$ mode and a $-$ mode) are

$$\lambda_\pm = \mathrm{e}^{\pm\mathrm{i}\phi} \quad , \quad \sin\frac{\phi}{2} = \frac{\Upsilon}{2} \, , \qquad (11)$$

with eigenvectors

$$V_\pm = \begin{bmatrix}\pm\mathrm{e}^{\pm\mathrm{i}\phi/2}\\1\end{bmatrix} \, .$$

Stability requires $\phi = \mathrm{real}$, or

$$\Upsilon \le 2 \, .$$

For weak beams, $\Upsilon \ll 1$, we have $\phi \approx \Upsilon$. Near the instability, ϕ approaches π as Υ approaches 2.

After a moment of reflection, we see that the instability when $\Upsilon > 2$ causes a rather severe disruption of the beam, as seen by the fact that, during half a synchrotron period, the motion of the trailing particle has grown by an amount more than twice the amplitude of the free-oscillating leading particle. For $\Upsilon \le 2$, the growths made during the half synchrotron periods when the particle is trailing do not accumulate and the beam is stable. As the beam intensity increases so that $\Upsilon > 2$, the growths of the particles then do accumulate and bootstrap into an instability. This *threshold* behaviour is very different from the linac case, in which the beam head is always stable and the beam tail is always unstable. One can imagine that, by periodically exchanging the roles of leading and trailing particles, the two-particle beam is made more stable. The more frequently the roles are exchanged, the more stable is the beam, as evidenced by $\Upsilon \propto 1/\omega_\mathrm{s}$. Synchrotron oscillation is thus an effective stabilizing mechanism in circular
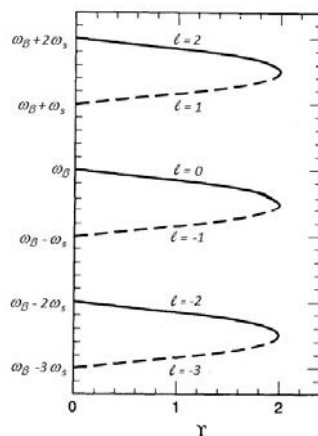
Fig. 18: Solid curves are the spectrum of the + mode; dashed curves are that of the − mode. Instability occurs at the point where the mode frequencies merge.

accelerators. Strong betatron focusing and a high beam energy also help stabilize the beam, as indicated by $\Upsilon \propto 1/(\gamma \omega_\beta)$.

In an accelerator, the beam signal comes from the beam position monitors that detect the centre of charge $y_1 + y_2$ of the beam, and it would be useful to examine its frequency spectrum. To do that, consider a two-particle beam in a pure eigenstate $V_\pm$ at time $s/c = 0$. In the stable region, the subsequent motion of the beam centre of charge is

$$(\tilde{y}_1 + \tilde{y}_2)(s) = \exp\left[-i\left(\omega_\beta \mp \frac{\phi\omega_s}{2\pi}\right)\frac{s}{c}\right] \sum_{\ell=-\infty}^{\infty} C_\ell e^{-i\ell\omega_s s/c} ,$$

$$C_\ell = 2i\Upsilon \frac{1 \pm (-1)^\ell}{(2\pi\ell \mp \phi)^2}(1 \mp e^{\pm i\phi/2}) .$$

The $\pm$ modes as observed by a beam position monitor therefore contain the following frequencies:

$$+ \text{mode:} \quad \omega_\beta + \ell\omega_s - \frac{\phi}{2\pi}\,\omega_s , \quad \ell = \text{even} ,$$

$$- \text{mode:} \quad \omega_\beta + \ell\omega_s + \frac{\phi}{2\pi}\,\omega_s , \quad \ell = \text{odd} .$$

Note that each mode contains a multiplicity of frequencies when observed continuously in time.

For weak beams, the two macroparticles oscillate in phase in the + mode and out of phase in the − mode. As Υ increases, the mode frequencies shift and the particle motions become more complicated; each mode contains a combination of in-phase and out-of-phase motions. At the stability limit $\Upsilon = 2$, the frequencies of the two modes merge into each other and become imaginary, which means instability (Fig. 18).

To detect internal beam motion in addition to the centre of charge motion, one uses a streak camera. One such observation, made on the large electron–positron collider at CERN, is shown in Fig. 19. It shows the turn-by-turn pictures of a beam executing a transverse head–tail oscillation. The bunch is seen from the side and one observes a vertical head–tail oscillation ($\ell = 1$). The horizontal scale is 500 ps for the total image. The vertical scale is uncalibrated. Figure 19 shows the same bunch each turn from top to bottom.

The strong head–tail instability is one of the cleanest instabilities that can be observes in electron storage rings. One can measure the threshold beam intensity when the beam becomes unstable
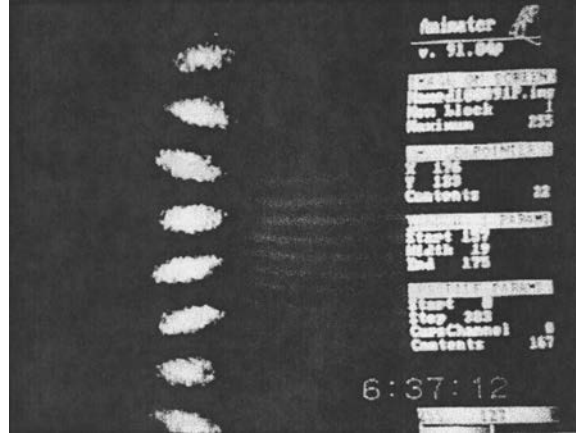
Fig. 19: Beam executing a transverse head–tail oscillation (Courtesy Albert Hofmann and Edouard Rossa, 1992)

transversely and associate the observation with $\Upsilon = 2$. Another approach is to measure the 'betatron frequency' (what is measured is the frequency of the $\ell = 0$ spectral line) as the beam intensity is varied. From our two-particle analysis, the initial slope of this frequency shift is

$$\left(\frac{\mathrm{d}\omega_\beta}{\mathrm{d}N}\right)_{N=0} = -\frac{\omega_\mathrm{s}}{2\pi}\left(\frac{\mathrm{d}\phi}{\mathrm{d}N}\right)_{N=0} = -\frac{r_0 W_0 c^2}{8\gamma C\omega_\beta} \ .$$

By measuring the instability threshold or the initial slope of the betatron frequency, information on the short-range wakefield or broad-band impedance can be obtained.

At the instability threshold, the measured betatron frequency has shifted by $\omega_\mathrm{s}/2$, according to the two-particle model. The measured value of $(\mathrm{d}\omega_\beta/\mathrm{d}N)_{N=0}$ can be used to predict the instability threshold N_th by

$$N_\mathrm{th} = -\frac{\omega_\mathrm{s}}{\pi}\frac{1}{(\mathrm{d}\omega_\beta/\mathrm{d}N)_{N=0}} \ .$$

The eventual instability threshold can thus be estimated by measuring ω_β at low beam intensities.

The two-particle model also predicts that the $\ell = 0$ frequency always shifts *down* as the beam intensity is increased. Physically, this is because, for short bunches, the sign of the wake force is such that the bunch tail is always deflected further away from the vacuum chamber axis if the beam is transversely displaced. With the head and the tail moving together in the $\ell = 0$ mode, the wake force acts as a defocusing effect and the mode frequency shifts down.

The centre of charge signal of the beam as a function of time after the beam receives an initial transverse kick can be analysed for a two-particle model. Figure 20 shows a result compared with experimental observation at PEP. The agreement indicates that the highly idealized two-particle model describes this instability mechanism remarkably well. The signal exhibits damping because of radiation damping.

19 Landau damping

Many collective instability mechanisms act on a high-intensity beam in an accelerator, demanding a wide range of sometimes conflicting stability conditions. Yet the beam as a whole seems basically stable, as evidenced by the existence of a wide variety of working accelerators. One reason for this fortunate outcome is *Landau damping*, which provides a natural stabilizing mechanism against collective instabilities, if particles in the beam have a small spread in their natural (synchrotron or betatron) frequencies.

The spread in ω_β has several sources. A dependence of ω_β on the energy of the particle, together with an energy spread in the beam, leads to a spread in ω_β. Non-linearities in the focusing system cause
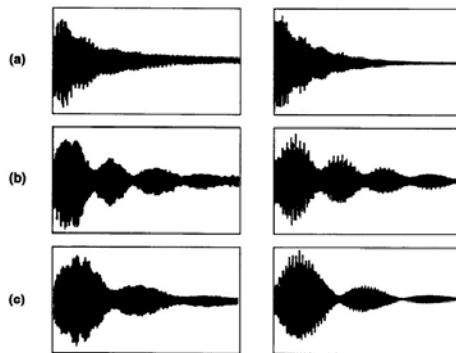
Fig. 20: Beam position monitor signal as a function of time after the beam is kicked. Left: PEP data with (a) $N/N_{\text{th}} = 0.86$, (b) $N/N_{\text{th}} = 0.93$, and (c) $N/N_{\text{th}} = 0.988$. Right: two-particle model with (a) $\Upsilon/2 = 0.77$, (b) $\Upsilon/2 = 0.96$, and (c) $\Upsilon/2 = 0.99$.

a dependence of ω_β on the particle's betatron amplitude. A spread in betatron amplitudes then leads to a spread in ω_β.

The source of spread in ω_s depends on whether the beam is bunched or unbunched. For bunched beams, a spread can result from non-linearity in the RF focusing voltage. For unbunched beams, the dependence of the revolution frequency on the particle energy plays a similar role.

Consider a simple harmonic oscillator with natural frequency ω driven by a sinusoidal force of frequency Ω,

$$\ddot{x} + \omega^2 x = A \cos \Omega t ,$$

with initial conditions $x(0) = 0$ and $\dot{x}(0) = 0$. The solution is

$$x(t > 0) = -\frac{A}{\Omega^2 - \omega^2}(\cos \Omega t - \cos \omega t) . \tag{12}$$

The $\cos \Omega t$ term gives the main term responding to the driving force; the $\cos \omega t$ term comes from matching the initial conditions.

The explicit inclusion of the initial conditions plays an important role. Otherwise, one could have carelessly written the solution

$$x(t) = -\frac{A}{\Omega^2 - \omega^2} \cos \Omega t, \quad \text{or} \quad x(t) = -\frac{A}{\Omega^2 - \omega^2} e^{-i\Omega t} . \tag{13}$$

Equation (13) contains a singularity at $\Omega = \omega$, while Eq. (12) is well behaved there. This singularity is the source of subtleties and at this point is to be avoided. As we will see later, by applying some mathematical tricks, it is possible to bypass the explicit inclusion of the initial conditions and go straight to Eq. (13) but at this point we will stay with Eq. (12).

Consider now an ensemble of oscillators (each oscillator represents a single particle in the beam) which have a spectrum $\rho(\omega)$ satisfying $\int_{-\infty}^{\infty} d\omega \rho(\omega) = 1$. Now subject this ensemble of particles to the driving force $A \cos \Omega t$ with all particles starting with initial conditions $x(0) = 0$ and $\dot{x}(0) = 0$. The ensemble average response is

$$\langle x \rangle(t > 0) = -\int_{-\infty}^{\infty} d\omega \rho(\omega) \frac{A}{\Omega^2 - \omega^2}(\cos \Omega t - \cos \omega t) .$$

For simplicity, let us consider a narrow beam spectrum around a frequency ω_x and a driving frequency near the spectrum, i.e., $\Omega \approx \omega_x$. The beam response is then

$$\langle x \rangle(t) = -\frac{A}{2\omega_x} \int_{-\infty}^{\infty} d\omega \rho(\omega) \frac{1}{\Omega - \omega}(\cos \Omega t - \cos \omega t) .$$
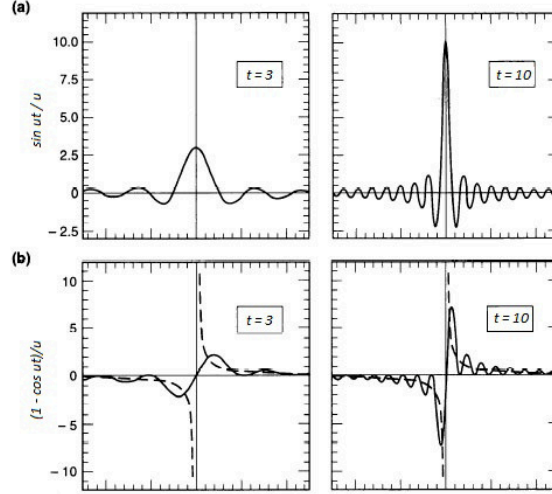
Fig. 21: The functions $\sin(ut)/u$, $(1 - \cos ut)/u$ are shown in (a), (b) for two values $t = 3$ and 10. The dashed curves in (b) are for the function $1/u$. The sole function of $(1 - \cos u)$ in (b) is to suppress the singularity at $u = 0$.

Changing variable from ω to $u = \omega - \Omega$ leads to

$$\langle x \rangle(t) = \frac{A}{2\omega_x} \int_{-\infty}^{\infty} du \frac{\rho(u + \Omega)}{u} [\cos \Omega t - \cos(\Omega t + ut)]$$

$$= \frac{A}{2\omega_x} \left[\cos \Omega t \int_{-\infty}^{\infty} du \rho(u + \Omega) \frac{1 - \cos ut}{u} + \sin \Omega t \int_{-\infty}^{\infty} du \rho(u + \Omega) \frac{\sin ut}{u} \right] .$$

All integrals are well behaved at $u = 0$.

The beam response contains a $\cos \Omega t$ term and a $\sin \Omega t$ term, but their coefficients are time dependent. The next step is to show that those coefficients approach well behaved limits. To do so, one first observes

$$\lim_{t \to \infty} \frac{\sin ut}{u} = \pi \delta(u) ,$$

$$\lim_{t \to \infty} \frac{1 - \cos ut}{u} = \text{P.V.} \left(\frac{1}{u} \right) .$$

The proof is illustrated in Fig. 21.

If we are not interested in the transient effects immediately following the onset of the driving force, we obtain

$$\langle x \rangle(t) = \frac{A}{2\omega_x} \left[\cos \Omega t \, \text{P.V.} \int d\omega \frac{\rho(\omega)}{\omega - \Omega} + \pi \rho(\Omega) \sin \Omega t \right] .$$

This expression explicitly contains a $\cos \Omega t$ term and a mysterious $\sin \Omega t$ term.

The sign of the $\cos \Omega t$ term relative to the driving force depends on the sign of P.V.$\int d\omega \rho(\omega)/(\omega - \Omega)$. A system is referred to as 'capacitive' or 'inductive' based on whether its sign is positive or negative.

The $\sin \Omega t$ term has a definite sign relative to the driving force because $\rho(\Omega)$ is always positive. In particular, $d\langle x \rangle/dt$ is always in phase with the force, indicating that work is being done on the system. The system always reacts to the force 'resistively'.

To proceed, write the beam response in complex notation,

$$\text{driving force} = Ae^{-i\Omega t} ,$$
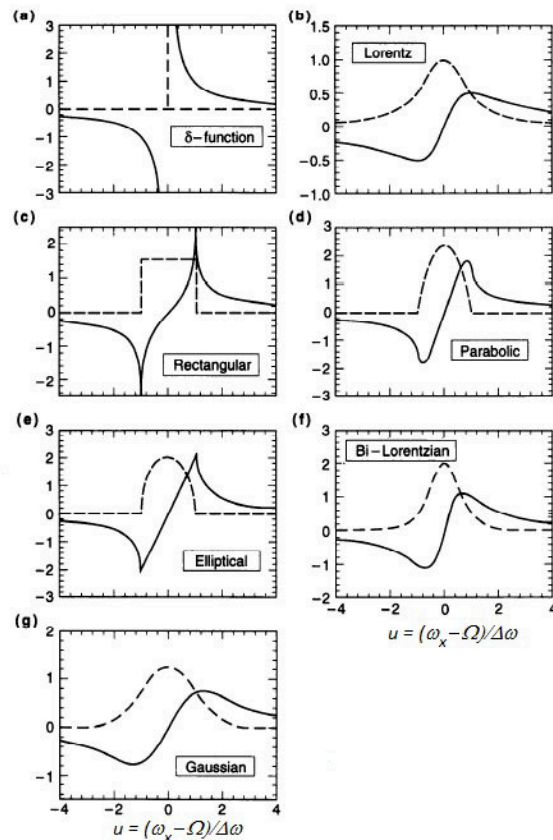
Fig. 22: The functions $f(u)$ (solid curves) and $g(u)$ (dashed curves) for various spectral distributions

$$\langle x \rangle = \frac{A}{2\omega_x \Delta\omega} e^{-i\Omega t} \left[f(u) + ig(u) \right] ,$$

where $u = (\omega_x - \Omega)/\Delta\omega$ with $\Delta\omega$ the width of the spectral spread, and

$$f(u) = \Delta\omega \; \text{P.V.} \int d\omega \frac{\rho(\omega)}{\omega - \Omega} ,$$

$$g(u) = \pi \Delta\omega \, \rho(\omega_x - u\Delta\omega) .$$

The dimensionless complex quantity $f + ig$ is the *beam transfer function* (Fig. 22).

For the δ-function spectrum, there is no frequency spread, Landau damping is lost,

$$f(u) = \frac{1}{u}, \quad \text{and} \quad g(u) = \pi \delta(u) .$$

For the Lorentz spectrum,

$$f(u) = \frac{u}{1 + u^2}, \quad \text{and} \quad g(u) = \frac{1}{1 + u^2} .$$

We now introduce a mathematical trick. It turns out that one can 'derive' the same result by venturing with Eq. (13). In complex notation, Eq. (13) gives

$$\langle x \rangle = \frac{A}{2\omega_x} e^{-i\Omega t} \int d\omega \frac{\rho(\omega)}{\omega - \Omega} .$$
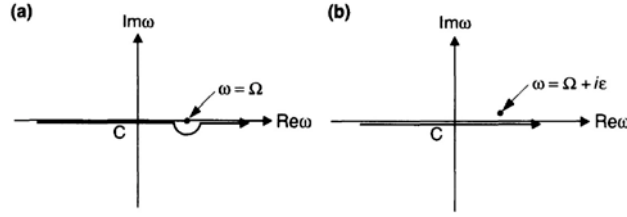
Fig. 23: Contour of integration

Our detailed examinations provides a well defined way to deal with the otherwise undefined integral, i.e.,

$$\int \mathrm{d}\omega \frac{\rho(\omega)}{\omega - \Omega} \quad \rightarrow \quad \mathrm{P.V.} \int \mathrm{d}\omega \frac{\rho(\omega)}{\omega - \Omega} + \mathrm{i}\pi\rho(\Omega) \,, \tag{14}$$

or, more symbolically,

$$\frac{1}{\omega - \Omega} \quad \rightarrow \quad \mathrm{P.V.}\left(\frac{1}{\omega - \Omega}\right) + \mathrm{i}\pi\delta(\omega - \Omega) \,.$$

Again, it is necessary to include an out-of-phase term—with a definite sign—as evidenced by the imaginary term $\mathrm{i}\pi\rho(\Omega)$, even though the expression on the left-hand side seems to be for a real quantity.

The right-hand side of Eq. (14), in fact, is equal to the left-hand side, provided one takes the integration to be executed in the complex ω-plane and the contour of integration, C, is as illustrated in Fig. 23(a). The connection (Eq. (14)) now reads

$$\int \mathrm{d}\omega \frac{\rho(\omega)}{\omega - \Omega} \quad \rightarrow \quad \int_C \mathrm{d}\omega \frac{\rho(\omega)}{\omega - \Omega} \,.$$

The straight line portion of C gives the principal value term in $\langle x \rangle$ and the semicircular portion gives the pole contribution $\mathrm{i}\pi\rho(\Omega)$.

Equivalently, one could consider the integration along the real axis of the ω-plane, but move the pole at $\omega = \Omega$ up by an infinitesimal amount,

$$\int d\omega \frac{\rho(\omega)}{\omega - \Omega} \quad \rightarrow \quad \int_{-\infty}^{\infty} \mathrm{d}\omega \frac{\rho(\omega)}{\omega - \Omega - \mathrm{i}\epsilon} \,,$$

or

$$\frac{1}{\omega - \Omega} \quad \rightarrow \quad \frac{1}{\omega - \Omega - \mathrm{i}\epsilon} \,,$$

or simply

$$\Omega \quad \rightarrow \quad \Omega + \mathrm{i}\epsilon \,. \tag{15}$$

It is now a matter of taste whether to regard our main conclusion (Eq. (14)) as a result of a simple derivation starting with Eq. (13) and then make a profound connection (Eq. (15)), or to regard it as a result of a detailed calculation that takes initial conditions into account.

20 One-particle model for bunched beams – transverse

The results obtained in the previous section applied to circular accelerators lead to Landau damping of collective instabilities. To demonstrate this for a bunched beam, consider a one-particle model, except that now the N individual particles have a spread in their natural frequencies. The fact that they form one macroparticle even though they have different frequencies is a result of the bunch executing a collective motion.

The driving force on the individual particles comes from the centre of charge displacement of the beam as a whole, $\langle y \rangle$, through the wakefield. For a single particle whose betatron frequency is ω,

$$y''(s) + \left(\frac{\omega}{c}\right)^2 y(s) = -\frac{Nr_0}{\gamma C} \sum_{k=1}^{\infty} \langle y \rangle (s - kC) \, W_1(-kC) \,,$$

Consider the situation when y-motion of the macroparticle is just at the edge of exponential growth, owing to a collective instability. We have

$$\langle y \rangle (s) = B\mathrm{e}^{-\mathrm{i}\Omega s/c} \,, \tag{16}$$

where Ω carries an imaginary part $\mathrm{i}\epsilon$, where ϵ is infinitesimally positive.

It is not very interesting to search for damped, stable solutions. Finding stable solutions does not assure beam stability, but finding one unstable solution reveals the beam to be unstable.

We now have

$$y''(s) + \left(\frac{\omega}{c}\right)^2 y(s) = -\frac{BNr_0}{\gamma C} \mathcal{W}\mathrm{e}^{-\mathrm{i}\Omega s/c} \,,$$

where

$$\mathcal{W} = \sum_{k=1}^{\infty} W_1(-kC)\mathrm{e}^{\mathrm{i}\omega_\beta kT_0} \,,$$

or, in terms of impedance,

$$\mathcal{W} = -\frac{\mathrm{i}}{T_0} \sum_{p=-\infty}^{\infty} Z_1^{\perp}(p\omega_0 + \omega_\beta) \,.$$

We have assumed that the mode frequency shift is small so that $\Omega \approx \omega_\beta$, where ω_β is the centre of the beam frequency spectrum.

The beam is driven by a sinusoidal driving force. Our analysis of Landau damping gives the beam response,

$$\langle y \rangle = -\frac{BNr_0 \mathcal{W}c}{2\omega_\beta \gamma T_0}\mathrm{e}^{-\mathrm{i}\Omega s/c}\left[\mathrm{P.V.}\int \mathrm{d}\omega \frac{\rho(\omega)}{\omega - \Omega} + \mathrm{i}\pi\rho(\Omega)\right] \,.$$

But we had already assumed that the collective beam motion is given by Eq. (16). This means that the mode frequency Ω is not arbitrary. For the beam motion to be non-trivial, Ω must satisfy a self-consistency condition, the *dispersion relation*,

$$1 = -\frac{Nr_0 \mathcal{W}c}{2\omega_\beta \gamma T_0}\left[\mathrm{P.V.}\int \mathrm{d}\omega \frac{\rho(\omega)}{\omega - \Omega} + \mathrm{i}\pi\rho(\Omega)\right] \,,$$

or

$$-\frac{Nr_0 \mathcal{W}c}{2\omega_\beta \gamma T_0 \Delta\omega} = \frac{1}{f(u) + \mathrm{i}g(u)} \,.$$

If the beam does not have a natural frequency spread, we have $f(u) = 1/u$, $g(u) = 0$. The complex mode frequency shift is found to be

$$(\Omega - \omega_\beta)_{\text{no Landau damping}} = \frac{Nr_0 c\mathcal{W}}{2\omega_\beta \gamma T_0} \,.$$

We shall designate this quantity as ξ_1; it contains essentially the beam intensity, multiplied by the impedance, divided by the focusing strength and the magnetic rigidity.

For a beam with natural frequency spread, the dispersion relation is

$$-\frac{\xi_1}{\Delta\omega} = \frac{1}{f(u) + \mathrm{i}g(u)} \,. \tag{17}$$

The left-hand side of Eq. (17) contains information about the beam intensity and the impedance. The right-hand side contains information about the beam frequency spectrum. For a given impedance, the left-hand side is obtained by calculating the complex mode frequency shift ξ_1 in the absence of Landau damping. Without Landau damping, the stability condition is simply $\text{Im}\,\xi_1 < 0$.

Once its left-hand side is obtained, Eq. (17) can, in principle, be used to determine Ω in the presence of Landau damping when the beam is at the edge of instability. However, the exact value of Ω is not useful. The useful question to ask is under what conditions the beam becomes unstable, regardless of the exact value of Ω. Equation (17) can be used in a reversed manner to address this question. To do so, consider the real parameter $u = (\omega_\beta - \Omega)/\Delta\omega$ and observe the locus traced out in the complex $\mathcal{D}_1$-plane as u is scanned from ∞ to $-\infty$, where

$$\mathcal{D}_1 = \frac{1}{f(u) + ig(u)} \ .$$

This locus defines a *stability boundary diagram* (Fig. 24). The left-hand side of Eq. (17), a complex quantity, is then plotted in the complex $\mathcal{D}_1$-plane as a single point. If this point lies on the locus, it means the solution of Ω for Eq. (17) is real, and this ξ_1 value is such that the beam is just at the edge of instability. If it lies on the inside of the locus (the side that contains the origin of the $\mathcal{D}_1$-plane), the beam is stable. If it lies on the outside of the locus, the beam is unstable.

The dispersion relation is particularly simple for the Lorentz spectrum (Fig. 24(b)),

$$\Omega = \omega_\beta + \xi_1 - i\Delta\omega \ .$$

The stability condition $\text{Im}\,\Omega < 0$ therefore becomes

$$\text{Im}\,\xi_1 < \Delta\omega \ .$$

The fact that the stable region is always enlarged by the frequency spread demonstrates the Landau damping mechanism. Its origin can be traced back to the fact that $g(u)$ is always positive, which in turn comes from the fact that the beam continues to absorb energy from the driving force without having to let $\langle y \rangle$ grow.

For a given spectral shape, the tolerable $\xi_1 \propto \Delta\omega$; the larger the frequency spread, the stronger the Landau damping. For a given $\Delta\omega$, the effectiveness of Landau damping is different for different spectral shapes. The Lorentz spectrum, having a long distribution tail, is most forgiving, while the δ-function spectrum is not effective.

For practical accelerator operations, there may be information on the value of the half-width-at-half-height $\Delta\omega_{\frac{1}{2}}$, but not enough detailed information on the shape of the frequency spectrum. For those applications, we introduce a simplified stability criterion,

$$|\xi_1| = \frac{Nr_0 c}{2\omega_\beta \gamma T_0^2} \left| \sum_{p=-\infty}^{\infty} Z_1^\perp(p\omega_0 + \omega_\beta) \right| < \frac{1}{\sqrt{3}} \Delta\omega_{\frac{1}{2}} \ , \tag{18}$$

where the factor $1/\sqrt{3}$ is chosen so that it coincides with the semicircular portion of the boundary for the elliptical spectrum. The stability diagram of this simplified model is shown in Fig. 24(h).

Equation (18) says that if the mode frequency shift or growth rate, calculated without Landau damping, is larger than the frequency spread of the beam, Landau damping will not rescue the beam from instability.
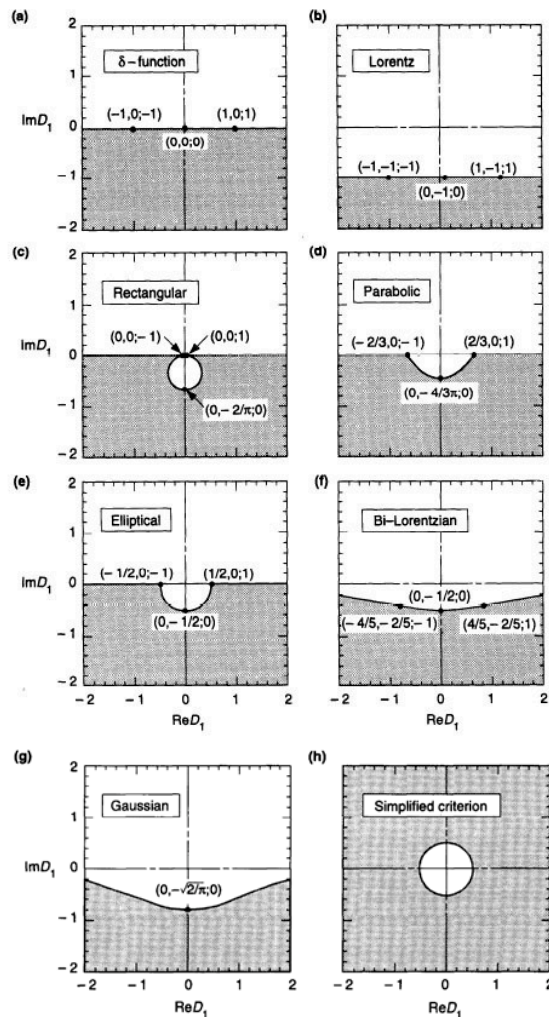
Fig. 24: The stability boundary diagrams for various spectra. Shaded regions are unstable. The coordinates labelled refer to $(\mathrm{Re}\mathcal{D}_1, \mathrm{Im}\mathcal{D}_1; u)$. The value of u can be used to obtain Ω. (a) δ-function spectrum, no Landau damping. (h) is the simplified criterion (Eq. (18)).

21 One-particle model for bunched beams – longitudinal

A similar analysis can also be performed for the longitudinal Robinson instability using a one-particle model,

$$z''(s) + \left(\frac{\omega_{\mathrm{s}}}{c}\right)^2 z(s) = \frac{Nr_0\eta}{\gamma C} \sum_{k=1}^{\infty} \left[\langle z\rangle(s) - \langle z\rangle(s - kC)\right] W_0''(-kC)$$

$$= \frac{Nr_0\eta}{\gamma C} B\mathrm{e}^{-\mathrm{i}\Omega s/c} \mathcal{W},$$

where we have introduced

$$\langle z\rangle(s) = B\mathrm{e}^{-\mathrm{i}\Omega s/c}$$

and

$$\mathcal{W} = \sum_{k=1}^{\infty} \left(1 - \mathrm{e}^{\mathrm{i}\omega_{\mathrm{s}}kT_0}\right) W_0''(-kC)$$

78

$$= \frac{\mathrm{i}}{C} \sum_{p=-\infty}^{\infty} \left[p\omega_0 Z_0^{\parallel}(p\omega_0) - (p\omega_0 + \omega_\mathrm{s}) Z_0^{\parallel}(p\omega_0 + \omega_\mathrm{s}) \right] \; .$$

Self-consistency then gives rise to a dispersion relation

$$\frac{N r_0 \eta \mathcal{W} c^2}{2\omega_\mathrm{s} \gamma C \Delta\omega} = \frac{1}{f(u) + \mathrm{i}g(u)} \; ,$$

similar to the transverse case except that the frequency spectrum now refers to synchrotron frequency, and the complex mode frequency shift in the absence of Landau damping is

$$\xi_1 = -\frac{N r_0 \eta \mathcal{W} c^2}{2\omega_\mathrm{s} \gamma C} \; .$$

The simplified stability criterion reads

$$|\xi_1| = \frac{N r_0 \eta c^2}{2\omega_\mathrm{s} \gamma C^2} \left| \sum_{p=-\infty}^{\infty} \left[p\omega_0 Z_0^{\parallel}(p\omega_0) - (p\omega_0 + \omega_\mathrm{s}) Z_0^{\parallel}(p\omega_0 + \omega_\mathrm{s}) \right] \right| < \frac{1}{\sqrt{3}} \Delta\omega_{\frac{1}{2}} \; .$$

The conclusion that the longitudinal Landau damping behaves analogously to the transverse case, however, is valid only for *bunched* beams for which $\omega_\mathrm{s} \neq 0$. The analyses depend on the assumption that the mode frequency shift $|\Omega|$ is small compared with the unperturbed natural frequency $\omega_\beta, \omega_\mathrm{s}$. For unbunched beams, $\omega_\mathrm{s} = 0$, the longitudinal analysis gives results very different from its transverse counterpart.